INSTITUTO TECNOLOGICO Y DE ESTUDIOS SUPERIORES DE MONTERREY

CAMPUS MONTERREY

GRADUATE PROGRAM IN MECHATRONICS AND INFORMATION TECHNOLOGIES

TECNOLÓGICO DE MONTERREY

DESIGN SPACE EXPLORATION AND SYNTHESIS OF A CMOS-MEMS Z-AXIS ACCELEROMETER

THESIS

PRESENTED AS A PARTIAL FULFILLMENT OF THE REQUIREMENTS FOR THE DEGREE OF

MASTER OF SCIENCE WITH MAJOR IN ELECTRONIC ENGINEERING (ELECTRONIC SYSTEMS)

BY

ALEJANDRO MENDEZ MORENO

MONTERREY, N. L. MEXICO DEC. 2010

INSTITUTO TECNOLOGICO Y DE ESTUDIOS SUPERIORES DE MONTERREY

MONTERREY CAMPUS

GRADUATE PROGRAM IN MECHATRONICS AND INFORMATION TECHNOLOGIES

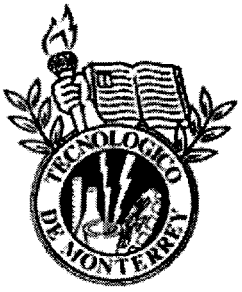

TECNOLÓGICO DE MONTERREY®

DESIGN SPACE EXPLORATION AND SYNTHESIS OF A CMOS-MEMS Z-AXIS ACCELEROMETER

THESIS

PRESENTED AS A PARTIAL FULFILLMENT OF THE REQUIREMENTS FOR THE DEGREE OF MASTER OF SCIENCE WITH MAJOR IN ELECTRONICS ENGINEERING (ELECTRONIC SYSTEMS)

BY

ALEJANDRO MENDEZ MORENO

MONTERREY, N.L., MEXICO DEC. 2010

INSTITUTO TECNOLOGICO Y DE ESTUDIOS SUPERIORES DE MONTERREY

MONTERREY CAMPUS

GRADUATE PROGRAM IN MECHATRONICS AND INFORMATION TECHNOLOGIES

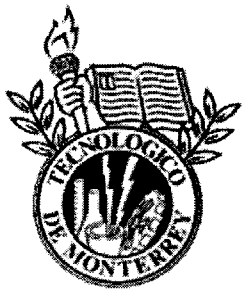

TECNOLÓGICO DE MONTERREY®

DESIGN SPACE EXPLORATION AND SYNTHESIS OF A CMOS-MEMS Z-AXIS ACCELEROMETER

THESIS

PRESENTED AS A PARTIAL FULFILLMENT OF THE REQUIREMENTS FOR THE DEGREE OF MASTER OF SCIENCE WITH MAJOR IN ELECTRONICS ENGINEERING (ELECTRONIC SYSTEMS)

BY

ALEJANDRO MENDEZ MORENO

MONTERREY, N.L., MEXICO DEC. 2010

DESIGN SPACE EXPLORATION AND SYNTHESIS OF A CMOS-MEMS Z-AXIS ACCELEROMETER

BY

ALEJANDRO MENDEZ MORENO

THESIS

PRESENTED TO THE GRADUATE PROGRAM IN MECHATRONICS AND INFORMATION TECHNOLOGIES

THIS THESIS IS A PARTIAL REQUIREMENT FOR THE DEGREE OF MASTER OF SCIENCE WITH MAJOR IN

ELECTRONICS ENGINEERING (ELECTRONIC SYSTEMS)

INSTITUTO TECNOLOGICO Y DE ESTUDIOS SUPERIORES DE MONTERREY

MONTERREY CAMPUS

DECEMBER, 2010

Acknowledgements

I would like to thank my advisor Professor Sergio Omar Martinez for his excellent guidance and support. He was always there when I needed to clarify any concept or to discuss a new idea. I would also like to thank Professor Alfonso Avila for his advice concerning this thesis and for the guidance he gave me as a teacher. I want to express my sincere thanks to Dr. Sergio Camacho and Dr. Fernando Alfaro, for sharing some of their great knowledge regarding MEMS with me and for giving me invaluable advice for my thesis.

I want to thank all the people at LabMEMS, for their friendship during these last two years.

Finally I want to thank my family for the love and support that they have given me throughout all my life.

Alejandro Méndez Moreno

Instituto Tecnológico y de Estudios Superiores de Monterrey
Dec, 2010

DESIGN SPACE EXPLORATION AND SYNTHESIS OF A CMOS-MEMS Z-AXIS ACCELEROMETER

Alejandro Méndez Moreno, M.S.
Instituto Tecnológico de Estudios Superiores de Monterrey, 2010

Thesis Advisor: Sergio Omar Martínez Chapa, Ph.D.

Abstract

This thesis presents a design space exploration of a CMOS-MEMS z-axis accelerometer and an approach towards the development of a synthesis procedure of this type of accelerometer.

In this work, a CMOS-MEMS z-axis accelerometer is designed and a series of equations to model its behavior are proposed. The accelerometer consists on a mechanical structure suspended on a silicon substrate that suffers a displacement upon certain acceleration. By using a capacitive interface, this displacement can be measured and the acceleration can be calculated. This accelerometer will be fabricated using a 0.35um CMOS process with three metal layers.

In the design space exploration, several dimensions of the designed accelerometer are varied over a range of values and the performance characteristics are obtained analytically using the proposed equations. The dimensions to be varied are the length and width of the beams of the spring system of the accelerometer, as well as the number of beams in the spring system. In order to validate the accuracy of the analytical results, the performance characteristics of each accelerometer structure are also obtained by system-level simulations performed using the Architect module of the Coventorware software suite. The maximum error between the analytic and the simulation results for the resonance frequency was 6.3%.

In the synthesis procedure presented, the dimensions of the spring system of the CMOS-MEMS accelerometer are modified automatically to meet a series of requirements specified by a user. The output of the synthesis program is the layout of the accelerometer, where the shapes of each layer of the CMOS process needed fabricate the structure are automatically generated. The performance of this synthesis program is verified by analyzing the generated structures with a FEM analysis using the Designer module of the Coventorware software suite. The maximum error between the synthesis program predictions and the FEM analysis results was 31% for the resonance frequency in the Z-axis.

Contents

List of Figures

List of Tables

Chapter 1

Introduction

Micro-electro-mechanical systems (MEMS) are devices that integrate mechanical and electrical components with dimensions in the micro or nano scale. Because MEMS allow the fabrication of very small and complex sensors and actuators, they have been widely used in industries such as the automotive and chemical industries.

Most of the technology that allows the fabrication of MEMS devices originates from the electronic industry. Since the invention of the transistor in 1947, the electronic industry has been continuously developing new techniques to achieve the integration of a higher number of electrical circuits in the smallest possible area, in order to produce smaller and more complex devices. These fabrication techniques have made possible the development of very powerful microprocessors like the Intel Core i7, which integrates approximately 731 million transistors in an area of only about 263 square millimeters [1]. This can be contrasted with the uP4004 microprocessor, developed in 1971, that integrated 2300 transistors in an area of 13.5 square millimeters [2].

The fabrication techniques of the electronic industry that allow this scale of miniaturization were adopted by the MEMS industry, modifying the processes that allowed the fabrication of very small transistors in a silicon chip in order to fabricate structures and components necessary to produce sensors and actuators.

One of the first applications of MEMS devices was their use in automobile impact sensors, used to detect collisions in vehicles and deploy the automobile's air bags when needed. MEMS devices were later used in electronic devices such as mobile phones and videogame consoles, in order to enhance the user's experience. More recently, MEMS devices have been used to detect the orientation and movement of the electronic devices so that the devices could interact with the user through these movements and changes in orientation. The iPhone 4, a mobile phone developed by Apple in 2010, includes a three axis MEMS accelerometer as well as a three-axis MEMS gyroscope, allowing the phone to detect linear and rotational movements in the three axes [3].

In the chemical industry, MEMS devices have encountered several applications; one of these has been its use in immunoassays. These biochemical tests have the purpose of measuring the concentration or presence of a determined substance in a solution, such as the level of hormones in a sample or the presence of virus or specific proteins. By detecting these substances,

sicknesses such as meningitis or hepatitis B can be diagnosed [4]. The use of MEMS devices has helped to increase the sensibility of the immunoassays, as well as decreasing the cost of the medical tests and allowing the application of several tests in parallel.

Recently, MEMS have found several applications in the medical industry. Among the products that use MEMS devices is the PocketCPR, which uses a MEMS accelerometer to measure the rhythm and depth of chest compressions administered by rescuers to patients [5]. Another product currently on the market is the Restoresensor neurostimulator, a device used to relieve pain and leg pain by delivering mild electrical signals to the spine [6]. This device uses a MEMS accelerometer to detect posture changes of the patients and with this information modulate and adjust the electrical signals delivered to the spine. These two products have something in common; the incorporation of a MEMS accelerometer.

An accelerometer is a transducer that converts the acceleration suffered by an object into another measurable variable, such as electrical current, voltage, magnetic field intensity, or a capacitance. Conventional accelerometers have dimensions that range in the order of several centimeters, which limits its use in mobile and medical applications. However, thanks to the development of MEMS technology in the last few years, accelerometers can now be fabricated inside an integrated circuit, occupying an area of less than 0.5 square millimeters. Because of their relatively low cost and excellent performance, MEMS accelerometers are now used in a wide range of devices, such as digital cameras, laptop computers, navigation systems and biomedical devices.

MEMS accelerometers can be fabricated using a great diversity of materials and the dimensions of each layer of these materials can be selected to satisfy the design requirements imposed by the designer. However, these customized process flows have a relatively high cost. Recently, a lot of interest has been placed in MEMS accelerometers that are fabricated using the CMOS process flow. The CMOS process is widely used in the electronic industry and integrated circuits using the CMOS technology can be fabricated at a relatively low cost. The accelerometers produced using the CMOS process flow are called CMOS-MEMS accelerometers. When designing these accelerometers, the restrictions of the CMOS process have to be taken into account. These restrictions include the materials that can be used, the height of each layer of material, the dimensions of each layer, etc. Besides from having a low cost, CMOS-MEMS accelerometers have the advantage of allowing an easier integration of the accelerometer and the circuits needed to amplify and modulate the electrical signals produced by the accelerometer.

1.1 Problem definition

Currently CMOS-MEMS accelerometers are designed in a process where the designer selects a topology among various pre-defined topologies and then starts modifying the dimensions of the accelerometer topology until the required characteristics are met. This process can take a considerable amount of time and the design of the accelerometer is done by a designer that must understand the details of operation of the accelerometer.

A synthesis procedure in which the layout of the accelerometer is automatically generated by taking as inputs the principal characteristics of the accelerometer would speed up the design process and would enable people who aren't very familiar with the operation and details of accelerometers to incorporate these inertial sensors in their designs.

Even though research involving synthesis procedures to automatically generate the layout of MEMS structures, including MEMS accelerometers, has been done before [7-14], a synthesis procedure focused on the synthesis of CMOS-MEMS accelerometers for out of plane acceleration measurement has not been reported yet.

In the current thesis, a design space exploration of a CMOS-MEMS z-axis accelerometer and an approach to the development of a synthesis technique for this accelerometer is presented. A MEMS accelerometer is composed of several subsystems; for the case of accelerometers with capacitive transduction, such as the one used in this thesis, these systems are the capacitive system, the spring system and the proof mass. Both the design space exploration and the synthesis technique in the current thesis will focus on the accelerometer's spring system.

The design space exploration will help us establish the relationships between the design variables of the accelerometer and the performance values of the spring system. The exploration will also help to establish the ranges of performance values that can be achieved.

The synthesis technique will allow users to specify the desired characteristics of the spring system of the accelerometer. Afterward, a layout of a CMOS-MEMS z-axis accelerometer meeting the user requirements can be generated.

1.2 Thesis Outline

In the second chapter of the current thesis, the state of the art of current CMOS-MEMS accelerometers and synthesis techniques of these devices is presented.

In the third chapter the CMOS process flow used to fabricate the accelerometer is presented.

The fourth chapter will introduce the basic concepts behind a MEMS accelerometer and its modeling.

The fifth chapter presents the design space exploration of a CMOS-MEMS accelerometer.

The sixth chapter details the synthesis method of the spring system of the CMOS-MEMS accelerometer.

Finally, in the seventh chapter the conclusions and references used in the current thesis are showed.

Chapter 2

State of the Art

In this chapter the state of the art regarding two topics of interest in the current thesis is presented. The chapter starts with a review in MEMS-based accelerometer and follows with a review in MEMS synthesis methods.

2.1 MEMS-based accelerometers

In the past few years, diverse structures for implementing MEMS accelerometers have been reported. Since the first MEMS accelerometer fabricated by Roylance in 1979, accelerometer structures and its fabrication processes have evolved, achieving better performance characteristics [15].

An accelerometer is basically composed of three subsystems, a proof mass, a spring system and a transduction system. MEMS accelerometers may be classified according to the transduction principle used or according to the fabrications technique used to construct them.

2.1.1 Transduction Principles

The most widely used transduction principles of MEMS accelerometers are piezoelectric, piezoresistive, capacitive and tunneling effect transduction.

Piezoelectric transduction is often used in applications where very high frequencies need to be measured and a good linearity is needed. Their principle of operation is the following, when an acceleration occurs, the proof mass of the accelerometer moves and causes a film of material located in the accelerometer springs to stress. This stress causes a potential difference between electrodes located in opposite sides of the film, and by measuring this electric potential difference the acceleration can be obtained. An example of an accelerometer using this type of transduction is the one fabricated by Hindrichsen et al. who reported a bulk-micro machined thin-film piezoelectric MEMS accelerometer that could measure accelerations having frequencies of up to 23.5 kHz and with a sensitivity of 0.24mV/g [16].

Piezoresistive transduction is relatively simple to implement, resulting in low cost devices. However their output voltage levels are relatively low, they have a considerable intrinsic

thermal noise and the output voltage does not have good thermal stability. These accelerometers are based on the fact that the resistance of polysilicon changes as a stress is applied to it, so by measuring the change in electrical resistance of a polysilicon film deposited in the spring beams suspending a proof mass, the acceleration can be measured. Haris et al. reported a CMOS-MEMS piezoresistive accelerometer with a 0.077mV/g sensibility consuming less than 1.5mW to operate [17].

Tunneling effect transduction offers the best sensibility of all transduction systems, but its implementation is much more complex and regularly needs manual assembly, so volume production is difficult in this moment. This accelerometer is based on the quantum mechanical phenomenon where a tunneling current flows between two structures separated by a very small distance even when the energy of the particles is less than the potential energy of the barrier between the structures. This current depends on the distance between the structures, so by measuring the current the distance between the proof mass and the substrate can be calculated. Haifeng et al. reported a MEMS tunneling accelerometer with a resolution of only 15 ug/$\sqrt{Hz}$ in the 1-100 Hz frequency range [18]. As a comparison, accelerometers having capacitive transduction regularly have a noise floor of 50-1000 ug/$\sqrt{Hz}$ [19-21].

Capacitive transduction offers an acceptable sensibility, suffers no significant output variations upon changes in temperature and is relatively easy to implement. This transduction technique relies on the measurement of the variation of electrical capacitance when the distance between two closely separated metallic structures changes. Capacitive transduction is used in the majority of MEMS accelerometers and will be used in the current thesis because of its good sensibility and its simple implementation using the CMOS process.

2.1.2 Fabrication Techniques

As mentioned before, MEMS accelerometers may also be classified according to the fabrication technology used. The two main categories of fabrication technologies are bulk micromachining and surface micromachining.

The first reported MEMS accelerometers were built using bulk micromachining. Bulk micromachining is a fabrication technique in which the shapes of the structures are formed by selectively etching the substrate. Bulk micromachining allows the fabrication of very thick structures. In the case of accelerometers this permits having very large proof masses and therefore high sensibility. However, structures built using this fabrication technique are not easily integrated with electronics. The structures reported in [15] and [16] were fabricated using bulk micromachining.

Surface micromachining is a fabrication technique based on the deposition and removal of thin layers of materials. In surface micromachining, the substrate is not affected, just the materials deposited on top of the substrate. Surface micromachining allows a better integration with microelectronics but has the disadvantage of not being able to fabricate thick structures. An example of an accelerometer fabricated with surface micromachining is the one reported by

Pakula et al. [22]. The sensitivity of this accelerometer has a value of 0.028mV/g, contrasting with the value of the bulk micro machined accelerometer reported by [16], which had a sensibility of 0.24mV/g.

A considerable number of accelerometers reported recently are built using the CMOS fabrication process. These accelerometers have the advantages of both techniques, a simpler integration with microelectronics and thick structures. The structures of these accelerometers are defined using the material layers of the CMOS process and afterwards the structure is released by a series of post-processing steps involving bulk micromachining, such as the accelerometer reported in [17].

2.1.3 Accelerometer Structures

Some of the latest MEMS accelerometer structures using a capacitive transduction will be presented in detail in the following paragraphs. There are two basic types of accelerometers, accelerometers that measure accelerations in the in-plane directions and accelerometers that measure accelerations in the out of plane direction, or Z-axis.

For the case of in-plane accelerometers, the structures reported in the past decade are somehow similar to the lateral accelerometer proposed by Luo et al. [19]. This structure basically consists of a central mass suspended by a crab shaped spring with a series of capacitive fingers attached to the mass and the substrate. The performance characteristics of this structure of accelerometer are very good for most applications. However, the reported structures for measuring the acceleration in the out-of-plane direction have been more diverse, each structure having certain advantages.

In 2008, Hongwei et al. reported an accelerometer structure for the sensing of the Z-axis which consisted in an imbalanced central mass, which in the presence of acceleration in the z-axis direction would make the mass rotate along a central axis [23]. The capacitive fingers attached to the ends of the rotating central mass move up or down with respect to the fixed fingers in the structure, so that the acceleration in the z-axis could be known measuring the change in capacitance between the fingers. A special fabrication process in which the back of the substrate is etched allowed the central mass to have a thickness of 50um.

This accelerometer structure not only measured accelerations in the out-of-plane axis, but also incorporated capacitive fingers and springs to measure accelerations in the X and Y axis. This structure had a total area of about 1.12 squared millimeters. The z-axis spring had a resonance frequency of 1.7kHz and a spring stiffness of about 1.13 N/m. The cross axis sensitivity reported for this accelerometer is 4.7%. The range of accelerations that it could measure is +/-50g. It was fabricated with a 0.35um TSMC technology.

Lemkin et al. fabricated a three axis accelerometer, with the advantage that the three accelerometers shared a single central mass [24]. In this type of structure the central mass is free to move in all directions and the capacitive fingers surrounding the central mass help to sense the

movement in the X and Y directions, while the Z-axis movement is sensed using a metal plate located beneath the central mass.

This accelerometer occupied an area of only 0.25 squared millimeters. The range of accelerations that the structure could sense is +/- 5.5g. The resonance frequency in the z-axis was 5.2kHz and it had a spring constant of about 0.4 N/m. The cross axis sensitivity reported was -39dB, or about 1.12%. This accelerometer was fabricated using a surface micromachining MEMS process.

Ming-Han et al. developed in 2008 a three axis accelerometer consisting of three separate accelerometers, one for each axis [25]. For the case of the accelerometer in the Z-axis, they used a central mass suspended by four springs, while lateral capacitive beams sensed the movement in the z-axis. These lateral capacitive beams were fabricated using a special procedure that allowed the finger capacitor gap to open and close in the z-axis direction.

Their accelerometer could measure accelerations in the range +/-6g in the z-axis. The resonance frequency and the stiffness in the z-axis direction were not reported. However, it was reported that the cross-axis sensitivity for this type of structure was in the range 15-30% a relatively high value. The accelerometer was fabricated using the 0.35um TSMC process.

In 2005, Junseok et al. reported a three axis accelerometer fabricated using both surface and bulk micromachining technology [26]. This allowed the central mass to have a thickness of 475um, very thick compared to other accelerometers. Not only the central mass, but also the capacitive fingers were thicker, so a bigger capacitive area and consequently a larger sensing capacitance was achieved.

For the case of the accelerometer in the z-axis, the stiffness constant of the spring system was 88 N/m, a relatively high value. But because of its very big mass, the resonance frequency had a value of only 100Hz. The z-axis accelerometer structure had an area of about 21 squared millimeters. Only accelerations in the range of +/-1g could be measured, but a high sensibility was obtained. The cross-axis sensibility was not reported.

In 2009, Sun et al. reported a three axis accelerometer where all three accelerometers shared the same surface area [27]. The fabrication process for the capacitive fingers was very similar to the one used in [25], but the shape of the springs of the suspension system where different in this case. The springs consisted of four long straight beams.

This accelerometer structure occupied an area of 0.592 squared millimeters. The reported value of the cross-axis sensitivity was 8.3%, much lower than the one reported in [25]. This accelerometer could measure a range of accelerations of +/-6g. The resonance frequency of the z-axis spring was 9.65kHz and the spring stiffness had a spring constant of about 4.36N/m. This accelerometer was fabricated using the 0.35 TSMC process.

Jung Tang et al. fabricated a z-axis accelerometer that had a sensing scheme similar to the one developed by Lemkin, in which the displacement of the central mass was measured using a capacitive plate located beneath the central mass [28]. The main difference is that Jung Tang fabricated this accelerometer using a conventional CMOS process, using a special post-

fabrication process afterwards to open the space between the central mass and the capacitive plate in the bottom.

Jung Tang's accelerometer could measure accelerations in a range of +/-10g. The resonance frequency of the spring system in the z-axis direction was 2.8kHz. The accelerometer structure occupied an area of 0.202 squared millimeters. The stiffness of the spring system was about 1.18 N/m. The technology used to fabricate this accelerometer was the 0.35 TSMC process.

In 2000, Huikai et al fabricated a z-axis accelerometer [29] using a similar structure and fabrication procedure as in [19]. The differences lie in the shape and dimensions of the spring system, that allow a much lower stiffness value in the z-axis direction, and in the way the capacitive fingers are connected.

The accelerometer reported by Huikai had a resonance frequency of 9.3kHz in the z-axis. It occupied an area of 0.25 squared millimeters. It was reported that its cross sensitivity was about -40dB, or 1%. The stiffness of the spring system has a value of about 1.76N/m. The range of acceleration that can be measured is +/-27g. The accelerometer was fabricated using the 0.5um Hewlett Packard CMOS process.

An example of an accelerometer currently in the market is the ADXL325 MEMS 3-axis accelerometer released in 2009 by Analog Devices [30]. This accelerometer has a resonance frequency of 5.5kHz in the z-axis and a cross-axis sensitivity of 1%. The range of acceleration that can be measured is +/-6g. The structure is fabricated using surface micro machining. No information about the total area of the accelerometer or the stiffness of the spring system is given.

STMicroelectronics has a family of MEMS inertial sensors, including the LIS344AL 3-axis accelerometer, fabricated using a CMOS process [31]. The resonance frequency in the z-axis of this accelerometer is 2 kHz, it can sense accelerations in the range +/-3.5g and it has a cross-axis sensitivity of 2%. No details on the spring stiffness in the Z-axis or area are given.

Table 2.1 summarizes the performance characteristics of the z-axis accelerometer structures mentioned in this section.

Table 2.1: Performance characteristics of reported Z-axis MEMS accelerometers

	Resonance frequency in the z-axis [kHz]	Maximum measurable acceleration range [g]	Stiffness in the Z-axis direction [N/m]	Cross-axis sensibility	Occupied Area [mm2]
Hongwei et al. [23]	1.7	+/- 50	1.13	4.7%	1.12
Lemkin et al. [24]	5.2	+/- 5.5	0.4	1.12%	0.25
Ming-Han et al. [25]	-	+/- 6	-	30%	-
JunSeok et al.[26]	0.1	+/- 1	88	-	21
Sun et al. [27]	9.65	+/- 6	4.36	8.3%	0.592
Jung Tang et al. [28]	2.8	+/- 10	1.18	-	0.202
Huikai et al [29]	9.3	+/- 27	1.76	1%	0.25
ADXL325 [30]	5.5	+/- 6	-	1%	-
LIS344AL [31]	2	+/- 3.5	-	2%	-

2.2 Synthesis of MEMS accelerometers

A considerable amount of research has been done to develop new fabrication processes and structures for MEMS devices. However, research regarding the synthesis of MEMS devices is still not abundant. The research in synthesis of MEMS can be divided in three main approaches, analytical model based synthesis, FEM model based synthesis and macro models or reduced-model synthesis.

Mukherjee et al. presented a synthesis method where the behavior of a MEMS microresonator was modeled by a series of equations obtained analytically [7]. Afterwards, the design problem was treated as a numerical optimization problem. It was reported that the structures resulting from this synthesis process had an error ranging in 22% to 30% in the resonance frequency when compared with FEM simulations, due to process variations that had not been incorporated in the analytical model.

Afterwards, a similar approach was taken by Mukherjee et al. [8] in order to develop a synthesis method for lateral MEMS accelerometers fabricated by the MUMPs process. It was reported that the spring stiffness and the resonance frequencies of the accelerometers had a maximum error of 5% when compared with FEM simulations, and a maximum error of 6% in predicting the cross-axis stiffness coupling in the X and Y directions.

Vishal Gupta developed a technique for synthesis of a lateral CMOS accelerometer in which both an analytical approach and a FEM simulation approach were made [9]. In the analytical approach, the accelerometer was modeled using a series of equations and then a non-

linear constrained optimization problem was formulated. In the FEM simulation approach, an annealing-based search was used to find the optimal design. A maximum error of 10% existed between the FEM simulations and the analytical approach regarding the mechanical part. It was reported that the FEM synthesis approach did function correctly and the structures were found, but it took a complete night to run the required simulations.

Younis et al. presented a reduced order macromodel of electrically actuated microbeam-based MEMS [10]. The simulation of this macromodel has a much lower computational cost that simulating the FEM structures. It was reported that the error between the macromodel and the FEM simulations was small, but no concrete values were given.

Kamalian et al. presented a FEM simulation based synthesis approach, using random walk functions and simulated annealing to synthesize a MEMS gyroscope [11]. It was reported that the synthesis tool took about 550 FEM simulations to reach the goal objectives.

Yang et al. reported a synthesis method based on metamodels [12]. This method consisted in first constructing the desired structure in a simulation software using a library of basic elements used in MEMS design, such as beams, anchors and plate masses. Then a series of simulations in which the dimensions of the basic elements that compose the structures are changed, and the performance variables of each structure are evaluated. Then, using this data, a metamodel of the variations of the performance variables with respect to the dimensions of the basic elements is developed. This metamodel is obtained using the optimization toolbox of Matlab. It was reported that the system is not very accurate, but the speed in which results can be obtained can make this system valuable in early stages of MEMS design.

Lo et. al reported the development of a software tool that implements a parameterized layout synthesis for MEMS and shows its application in MEMS resonators [13]. The method is based in solving a set of analytical equations to find the set of dimensions of the resonator that would satisfy the design parameters specified by the user. This tool was implemented in SPICE, so that a system including other electronic devices could be simulated along with the MEMS resonator.

Tran et al developed a method for the synthesis of a MEMS piezoresistive accelerometer using a combination of FEM simulation and modified modal analysis [14]. The synthesis method started by first using the modal analysis to analyze an initial structure and then perform an auto refinement by varying its dimensions. Afterwards, the structure could receive some manual tuning by the user. Finally the structure was subject to a FEM analysis. If the design conditions are not met, the structure goes into another similar loop until the conditions are met. This approach is faster than normal FEM simulation approaches because the FEM simulation is only done for the modal analysis verification. It was reported that the output between the simulated and the experimental values of an accelerometer fabricated using this synthesis method had an error of no more than 15%.

Chapter 3

Accelerometer Fabrication Process and Modeling

In the current chapter some necessary concepts related to the CMOS fabrication process, used to construct the CMOS-MEMS accelerometer, is presented. Afterwards, the basic theory for modeling the behavior of a MEMS accelerometer is explained.

3.1 Principal characteristics of the CMOS process

CMOS (Complementary Metal-Oxide-Semiconductor) is a technology used in the fabrications of electronic integrated circuits. Its name origins from the fact that both P and N type field effect transistors can be used when designing CMOS electronic circuits. Among the advantages of the CMOS technology when compared to electronic circuits fabricated using bipolar transistors is the low power consumption at low frequencies and the higher number of transistors that can be placed in an integrated circuit.

Because of these advantages, the CMOS technology has been widely used in the fabrication of electronic circuits such as microprocessors and RAM memory chips, where low power consumption and high transistor density are crucial factors for the performance of the circuits.

CMOS technology has evolved over time, allowing the fabrication of smaller transistors each time the fabrication processes improve. The main characteristic that can be used to classify different CMOS fabrication processes is the minimum length of the transistor gate that can be fabricated with a specific process. In the early 1990s, transistors with a gate of a length of 0.5 micrometers could be fabricated using CMOS technology. In 2009, new integrated circuits made of transistors having a gate's length as small as 30 nanometers were introduced into the market. Figure 2.1 shows a basic diagram of a CMOS transistor.

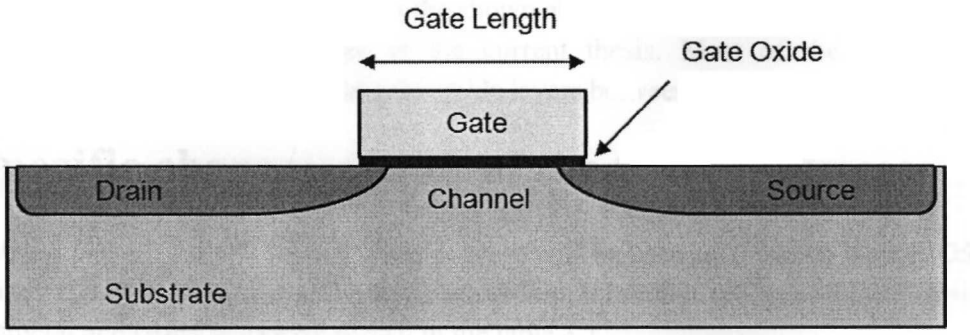

Figure 3.1: Diagram of a CMOS transistor

A CMOS transistor is composed of three electric terminals, called drain, source and gate. By interconnecting the terminals of CMOS transistors logic gates, memory banks, and other much more complex circuits can be formed. To interconnect the terminals of a CMOs transistor, various layers of metal are deposited above the transistors. These layers of metal have a bi-dimensional pattern that determines the connections between transistors. Additionally, connections between adjacent metal layers can be performed. Each metal layer is separated by an oxide layer in order to provide electrical insulation. In figure 2.2, a diagram representing a cross-section view of a silicon wafer after a 3 metal layer CMOS process is shown.

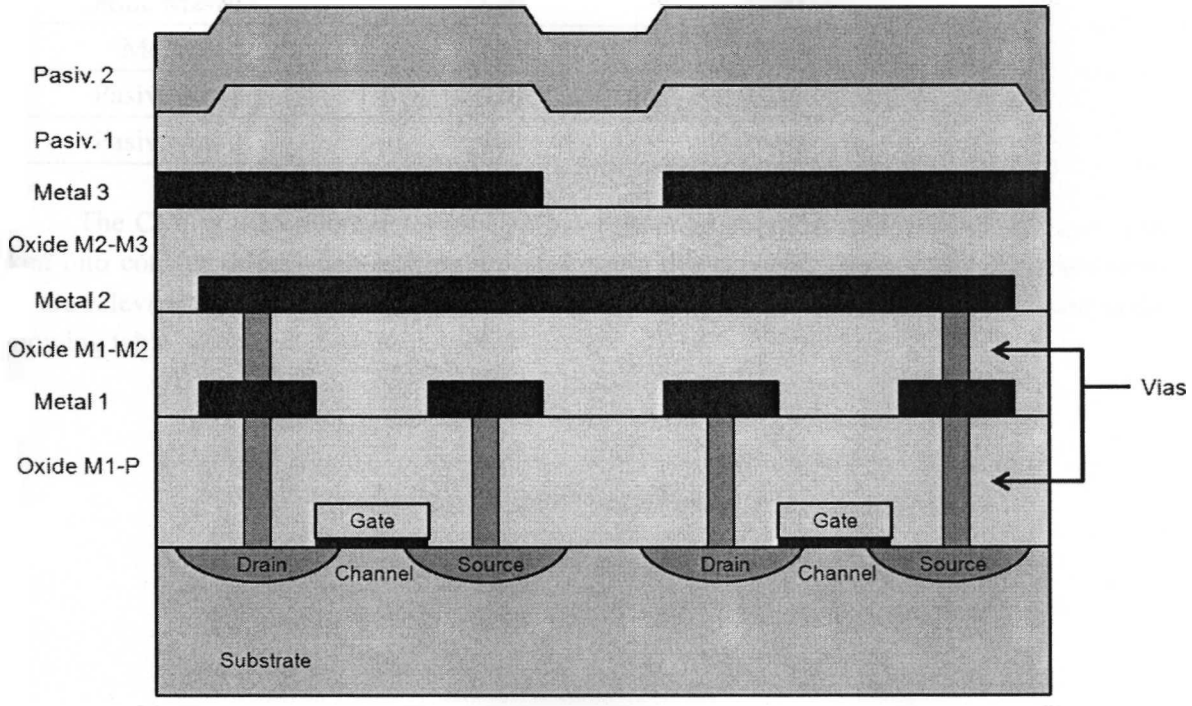

Figure 3.2: Cross-section view of a silicon wafer after 3 metal layer CMOS process

A 3 metal layer CMOS process as the shown above will be used to fabricate the structure of the CMOS-MEMS accelerometer in the current thesis. Most of the structure will be constructed using the 3 metal layers and the oxide layers between them.

3.2 Specific characteristics of the CMOS process

A commercial CMOS 0.35 micrometer process will be used to fabricate the CMOS-MEMS accelerometer. In this particular process, the maximum, minimum and typical thicknesses for the different metal and oxide layers are shown in the table 3.1.

Table 3.1: Thickness values for a metal and oxide layers in the CMOS 0.35 micrometer 3 layer process

	Minimum Thickness [nm]	Typical Thickness [nm]	Maximum Thickness [nm]
Oxide M1-P	395	645	895
Metal 1	565	665	765
Oxide M1-M2	620	1000	1380
Metal 2	540	640	740
Oxide M2-M3	620	1000	1380
Metal 3	775	925	1075
Pasivation 1	930	1030	1130
Pasivation 2	800	1000	1200

The CMOS 0.35 micrometer process has certain geometrical restrictions that have to be taken into consideration when making a design using this process. The geometrical restrictions that are relevant to the CMOS-MEMS accelerometer design in the current thesis are listed in the following table.

Table 3.2: Geometrical restrictions in the CMOS 0.35 micrometer 3 layer process

	Dimension [um]
Minimum width for Metal 1 layer	0.5
Minimum spacing between metal structures in Metal 1 layer	0.45
Minimum width for Metal 2 layer	0.6
Minimum spacing between metal structures in Metal 2 layer	0.5
Minimum width for Metal 3 layer	0.6
Minimum spacing between metal structures in Metal 3 layer	0.6
Via 1 minimum width	0.5
Minimum spacing between adjacent Vias 1	0.45
Minimum distance from end of metal to Via 1	0.2
Via 2 minimum width	0.5
Minimum spacing between adjacent Vias 2	0.45
Minimum distance from end of metal to Via 2	0.2

The geometrical restrictions for the CMOS process mentioned in the Table 3.2 are explained in diagram presented in Figure 3.3.

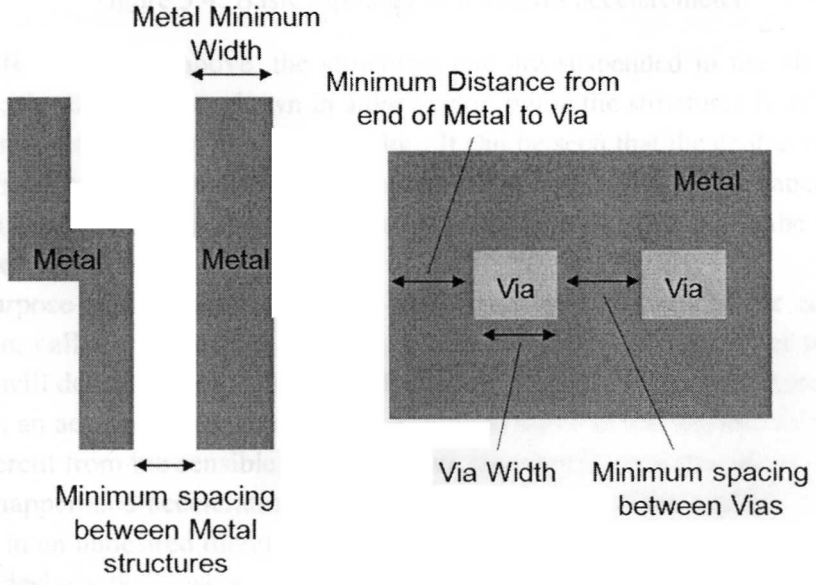

Figure 3.3: Geometrical constraints of metal and metal vias structures in the CMOS process.

3.3 Accelerometer modeling fundamentals

In this section the necessary concepts to model a MEMS accelerometer with a capacitive sensing system will be presented. As mentioned in section 2.1, a MEMS accelerometer basically consists of three main subsystems, a central mass, a spring system and a capacitive system. The basic structure of accelerometer for measuring the acceleration in the x-axis is shown below.

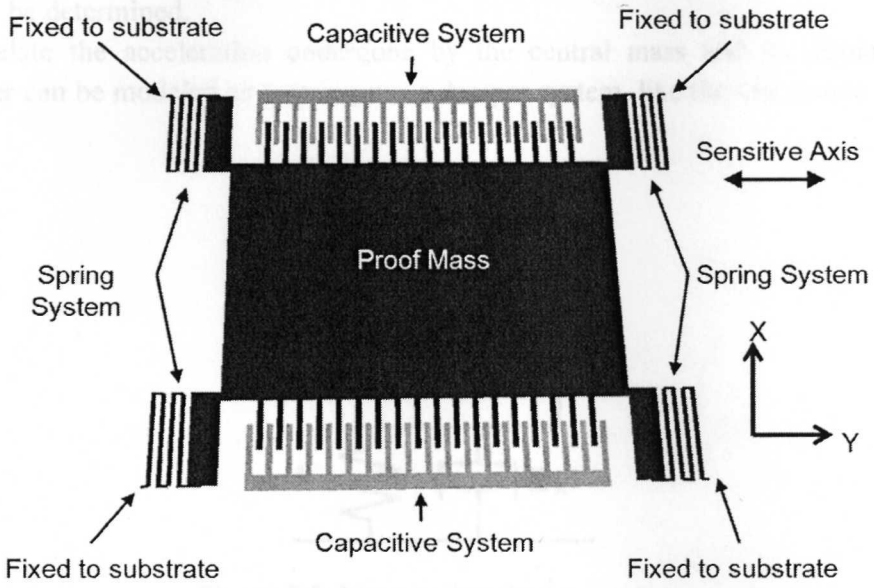

Figure 3.4: Basic topology of a MEMS accelerometer

In the figure shown above, the structures that are suspended in the air and are free to move in a specific direction are shown in a dark color, while the structures fixed to the substrate and unable to move are shown in a lighter color. It can be seen that the central mass is joined to the substrate by a series of beams that compose the spring system. The capacitive system is composed of a series of straight beams positioned in the central mass and in the substrate. These beams are called the capacitive fingers.

The purpose of the spring system is to restrict the movement of the central mass to a single direction, called the sensible axis. The arrangement and dimensions of the beams of the spring system will determine the stiffness of the spring system in each of the three axes.

Ideally, an accelerometer should only be able to move in the sensible axis, if acceleration in an axis different from the sensible axis is present, the central mass should not move. However, this does not happen and accelerations in a direction different of the sensible axis do move the accelerometer in an undesired direction. To compare this undesired movement between different spring system designs, the cross-axis sensibility is used.

To keep the value of the cross-axis sensibility as low as possible, the stiffness of the spring system in the directions that are not the sensible axis should be much larger than the stiffness of the spring system in the sensible axis.

The purpose of the capacitive system is to provide a way to measure the displacement of the central mass by giving an electrical output signal proportional to the displacement. This is done by measuring the change in capacitance between the capacitive fingers. By knowing the dimensions of these fingers and the variation in capacitance, the displacement suffered by the structure can be determined.

To relate the acceleration undergone by the central mass and its displacement, the accelerometer can be modeled as a spring-mass-damper system, like the one shown in the figure below.

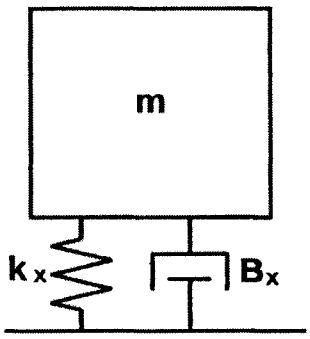

Figure 3.5: Mass-spring-damper system

In the case of a MEMS accelerometer, the mass "m" corresponds to the central mass, the mass of the capacitive fingers attached to the central mass and the effective mass of the spring beams in the spring system.

The damping constant "Bx" is calculated by taking into account the effect of Couette flow damping and the squeeze film damping. Couette flow damping occurs because of the shear flow of air between a pair of parallel surfaces, the substrate and the lower surface of the central mass in the case of the present accelerometer. Squeeze film damping occurs when the air gap between two closely positioned parallel surfaces changes.

The spring constant "kx" is obtained by calculating the stiffness of the spring system. The value of the spring constant, as well as the damping constant and the mass of the system is different for each direction.

Once these constants of the system are known, the magnitude of the displacement of the structure can be related to the acceleration using the following formula:

$$m\frac{dx^2}{dt^2} + b_x\frac{dx}{dt} + k_x x = ma_x \tag{3.1}$$

Using the Laplace transform on the previous equation, we can get an equation of the displacement in terms of the acceleration undergone by the structure.

$$\frac{X(s)}{A(s)} = \frac{1}{s^2 + s\frac{b_x}{m} + \frac{k_x}{m}} \tag{3.2}$$

The spring stiffness in the each direction can be obtained by first obtaining the resonance frequencies of the accelerometer structure in each direction. It is known that the resonance frequency of a mass-spring-damper system is related to the mass and spring constant using the following formula.

$$\omega_x = \sqrt{\frac{k_x}{m}} \tag{3.3}$$

So if we know the resonance frequency of the system for a specific direction, we can calculate the spring constant in that direction. The mass can be calculated by knowing the dimensions of the central mass, capacitive beams and spring beams of the accelerometer.

At frequencies much lower than the resonance frequency, s tends to zero and the mechanical sensitivity of the accelerometer can be approximated as

$$\frac{x}{a} = \frac{1}{\frac{k_x}{m}} = \frac{m}{k_x} \tag{3.4}$$

So having a bigger central mass or a smaller spring constant we can achieve a better mechanical sensitivity.

To measure the displacement of the central mass, the capacitive system generates a voltage signal proportional to the displacement. As it will be explained in the following chapter, the capacitive fingers can be connected in such a way to achieve a differential capacitive sensing, as shown in the figure below.

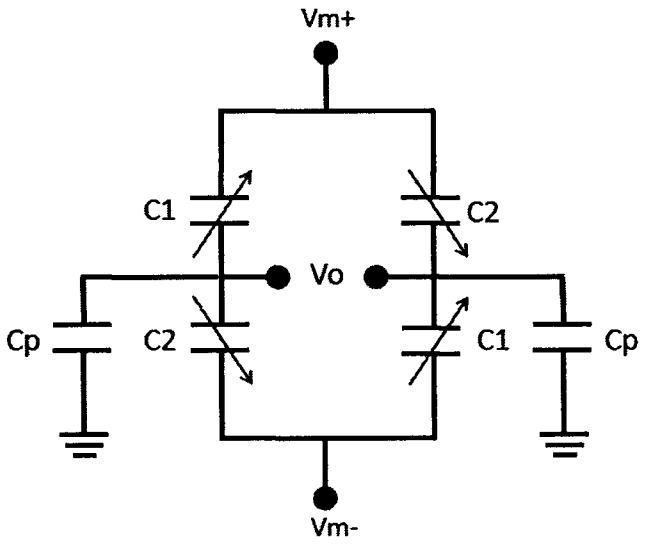

Figure 3.6: Differential-sensing capacitive system

The output voltage Vo can be related to the change of capacitance by the following formula,

$$V_o = \frac{2C_1 + 2C_2}{C_1 + C_2 + C_P} V_m \tag{3.5}$$

Where C_1 and C_2 represent the sensing capacitance between capacitive fingers and C_P stands for the parasitic capacitances. From this equation we can see that the capacitive system should have the biggest sensing capacitance possible to achieve a better sensibility when measuring accelerations.

Combining equations 3.4 and 3.5 and establishing a relationship between displacement and change in capacitance, a direct relationship between the accelerations and the output voltage may be obtained.

Chapter 4

CMOS-MEMS Accelerometer Design

In this chapter the steps followed to design a CMOS-MEMS accelerometer is explained. The first section explains the design procedure and modeling of the spring system. In the second section the capacitive system and its structure is detailed.

4.1 Design and modeling of the spring system

The accelerometer that was designed in this thesis is a out-of-plane accelerometer, which means that the accelerations to be measured will have its direction in the z-axis. The spring system in this type of accelerometer will have the purpose of permitting the accelerometer structure to move in the z-axis direction, while restricting the movement in the X-Y plane. This will be accomplished by having a spring system with a much higher stiffness in the X and Y axis directions compared to the stiffness in the Z-axis direction.

The topology of the spring system chosen to be used in the accelerometer will be based in a series of serpentine springs. The diagram of a system of four serpentine springs similar to the ones used in the accelerometer is shown in Figure 4.1.

This topology consists of two pairs of serpentine springs, a pair on each side of the proof mass. The beams in each pair of springs are symmetrical. Each serpentine spring consists of n + (n-1) beam segments, where n is the number of short spring beams. In this serpentine spring topology, the number of large spring beams will always be (n-1). In the figure 4.1, the n=3, the short spring beams consist of beams 1,3 and 5 while the long spring beams consist of beams 2 and 4. All the long spring beams and all the short spring beams will always have an equal length.

Because the beams 2 and 4 are considerably larger than the beams 1, 3 and 5, this type of serpentine spring has a much higher stiffness in the X axis compared to the stiffness in the Y-axis.

For the case of the spring system of figure 4.1, consisting of 4 serpentine springs, the stiffness in the Y axis can be calculated using the following equation [32],

$$k_c = \frac{48EI_{z,b}[(\tilde{a}+b)n-b]}{b^2(n-1)[(3\tilde{a}^2+4\tilde{a}b+b^2)n+3\tilde{a}^2-b^2]} \tag{4.1}$$

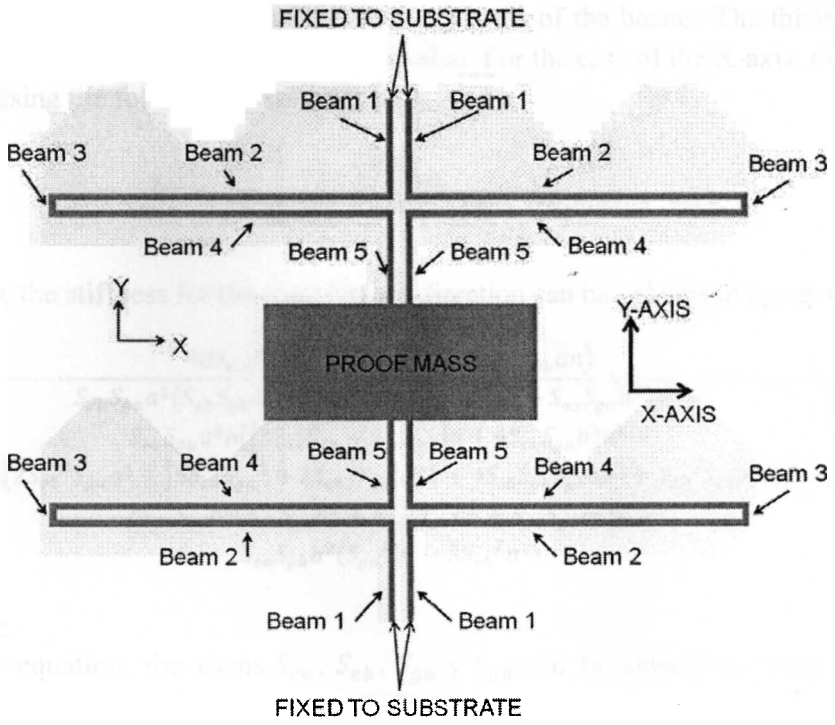

Figure 4.1: Spring system consisting in four serpentine spring segments.

In equation 4.1, E is the Young modulus of the material of the spring beams, $I_{z,b}$ is the moment of inertia of the long beams, a represents the length of the short spring beams and b represents the length of the long spring beams. In this equation, n represents the number of large spring beams in the system. The variable named $\tilde{a}$ stands for a relationship between the moment of inertia of the short spring beams and the long spring beams, and is calculated y the following equation,

$$\tilde{a} = \frac{I_{z,b}a}{I_{z,a}} \tag{4.2}$$

The moment of inertia for each type of beam can be calculated using equations 4.3 and 4.4,

$$I_{z,b} = \frac{{w_b}^3 t}{12} \tag{4.3}$$

$$I_{z,a} = \frac{{w_a}^3 t}{12} \tag{4.4}$$

Where w_b and w_a stand for the width of the long spring beams and the width of the short spring beams respectively and t stands for the thickness of the beams. The thickness of all the beams in the spring system will have the same value. For the case of the X-axis, the stiffness can be calculated using the following equation [32],

$$k_r = \frac{48EI_{z,b}}{a^2 n[(\tilde{a}+b)n^2 - 3bn + 2b]} \tag{4.5}$$

Finally, the stiffness for the out-of-plane direction can be calculated by equation 4.6 [32],

$$k_z = \frac{48S_{ea}S_{eb}S_{ga}S_{gb}(S_{ga}b(n-1)+S_{eb}an)}{\left(\begin{array}{c} S_{eb}S_{ga}a^2(S_{eb}S_{gb}a^2+[S_{ea}S_{eb}+S_{ga}S_{gb}]ab+S_{ea}S_{ga}b^2)n^4 - \\ S_{eb}S_{ga}a^2b([3S_{ea}S_{eb}+S_{ga}S_{gb}]a+4S_{ea}S_{ga}b)n^3 + \\ S_{ea}b(2{S_{eb}}^2S_{ga}a^3+[5S_{eb}{S_{ga}}^2+3{S_{eb}}^2S_{gb}]a^2b+4S_{eb}S_{ga}S_{gb}ab^2+{S_{ga}}^2S_{gb}b^3)n^2 - \\ 2S_{ea}S_{ga}b^2(S_{eb}S_{ga}a^2+2S_{eb}S_{gb}ab+S_{ga}S_{gb}b^2)n + \\ S_{ea}S_{gb}b^2({S_{ga}}^2b^2-3{S_{eb}}^2a^2) \end{array}\right)} \tag{4.6}$$

In this equation, the terms S_{ea}, S_{eb}, S_{ga} y S_{gb} can be calculated using the following equations.

$$S_{ea} = EI_{x,a} \tag{4.7}$$

$$S_{eb} = EI_{x,b} \tag{4.8}$$

$$S_{ga} = GJ_a \tag{4.9}$$

$$S_{gb} = GJ_b \tag{4.10}$$

The variable G represents the shear modulus of the material. The shear modulus of a material can be calculated using the Young modulus and the Poisson ratio v.

$$G = \frac{E}{2(1+v)} \tag{4.11}$$

Finally, the variables J_a and J_b represent the torsion consants of the short and long spring beams respectively. For the case of rectangular cross-section beams, J_a and J_b can be calculated using equations 4.12 and 4.13.

$$J_a = ab^3\left(\frac{1}{3} - 0.21\frac{b}{a}\left(1 - \frac{b^4}{12a^4}\right)\right) \tag{4.12}$$

$$J_b = ab^3\left(\frac{1}{3} - 0.21\frac{b}{a}\left(1 - \frac{b^4}{12a^4}\right)\right) \tag{4.13}$$

The equations above assumed the beams were made of a homogeneous material. In case the beams are made of more than one material, the Young modulus of the heterogeneous material will depend on the thickness of each of the materials and the Young modulus of each material.

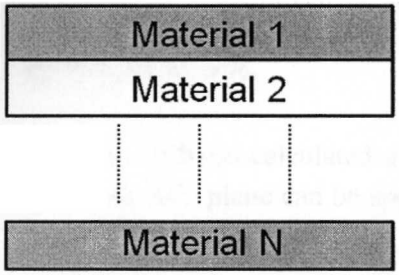

Figure 4.2: Beam composed of a stack of N materials

For the case of a beams compose of n layers of different materials, the Young modulus of the composite beams can be calculated by equation 4.14.

$$E = \frac{E_1 * t_1 + E_2 * t_2 + \cdots + E_n * t_n}{t_1 + t_2 + \cdots + t_n} \tag{4.14}$$

Where E_x and t_x represent the Young modulus and the thickness of material x respectively. The accelerometer to be designed in this thesis needs to be very stiff in the in the X and Y directions, while allowing movement in the Z-axis direction. To achieve that, an arrangement of 2 serpentine springs groups as the ones shown in figure 4.1 are used to suspend the proof mass of our accelerometer. The layout of the proposed design is shown in the figure below.

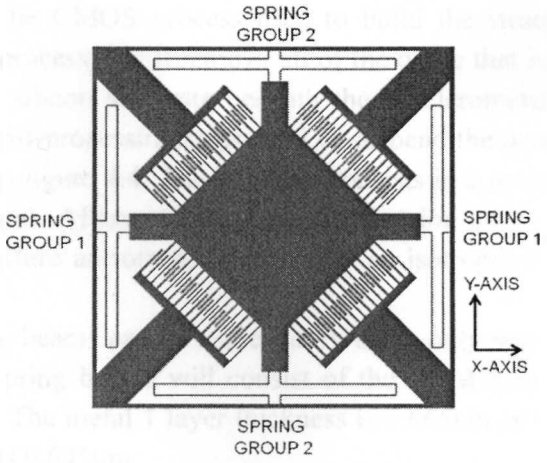

Figure 4.3: Proposed layout for the CMOS-MEMS accelerometer.

This topology consists of two serpentine spring groups. The first group contributes with a high stiffness in the Y axis, while spring group 2 contributes to a high rigidity in the X axis. For this particular design, assuming no fabrication variations in the spring beams, the stiffness in the X and Y directions are the same and are given by the following equation.

$$k_x = k_y = k_c + k_r \tag{4.15}$$

Where k_c and k_r correspond to the stiffness calculated using equations 4.1 and 4.5. The stiffness in an arbitrary direction inside the X-Y plane can be approximated making a projection of the stiffness on each axis.

$$k = k_c \cos\theta + k_c \sin\theta + k_r \cos\theta + k_r \sin\theta \tag{4.16}$$

The stiffness of the spring system in the z-axis is simply the sum of the stiffness of each group of springs.

$$k_{z\,tot} = 2k_z \tag{4.17}$$

In the design space exploration to be performed in the next chapter, some of the dimensions of the spring system will be varied while some other dimensions will be held constant.

One of the dimensions that will be held constant is the thickness of the beams of the spring system. In order to achieve a much lower stiffness in the Z-axis with respect to the in-plane stiffness, it is necessary to have the smallest value possible for the thickness of the spring beams.

The thickness of the beams of the spring system is determined by the materials used in the spring beams. After the CMOS process used to build the structure of the accelerometer finishes, some additional processes will remove all of the oxide that is not covered by metal and will remove some of the silicon substrate beneath the accelerometer structure to suspend the structure in the air. The post-processing steps used to suspend the accelerometer structure in the current thesis are shown in figure 4.4. The first step consists in a reactive ion etch to remove the oxide not covered by metal. Afterwards, a deep reactive ion etch is used to etch the silicon substrate beneath the structure anisotropically. Finally an isotropic silicon etch is performed to suspend the structure.

The thinnest spring beams can be achieved by using only metal 1 material for the spring beams. In this way, the spring beams will consist of the metal 1 layer material and the oxide beneath the metal 1 layer. The metal 1 layer thickness is 0.665um and the thickness of the oxide beneath the metal 1 layer is 0.645um.

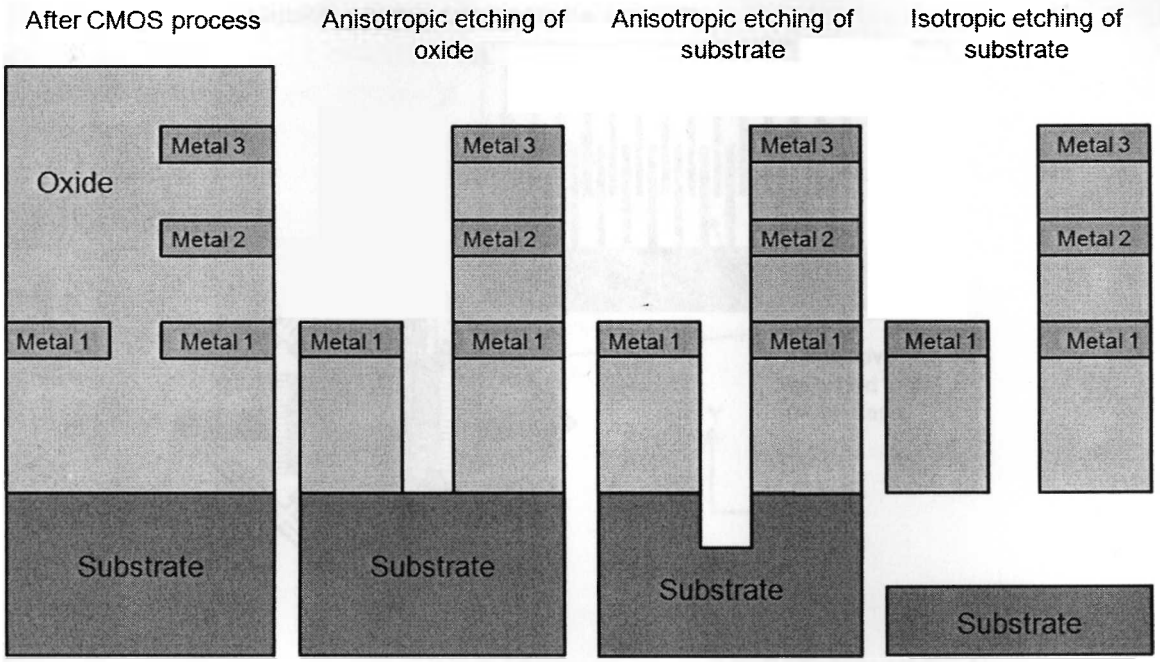

Figure 4.4 Post processing steps

Because of this undesired oxide, the spring beams will no longer be composed of a homogenous material and the equivalent Young modulus needs to be calculated. The aluminum of the metal layer has a Young modulus of 77GPa and a thickness of 0.665um, while the oxide has a Young modulus of 70GPa and a thickness of 0.645um. Having these values and using the equation 14, the equivalent Young modulus for the spring system beams can be calculated, giving a value of 73.55 GPa.

4.2 Capacitive Sensing System

The capacitive system of the accelerometer is used to convert the displacement of the proof mass of the accelerometer into a change in capacitance that can be measured using an electrical circuit that can be either external or incorporated into the accelerometer's integrated circuit.

The capacitive system consists in two groups of beams, one group placed in the perimeter of the proof mass and the other group of beams located in the substrate, as shown in figure 4.5. The beams attached to the proof mass will move along the proof mass, while the beams fixed to the substrate will not move at all.

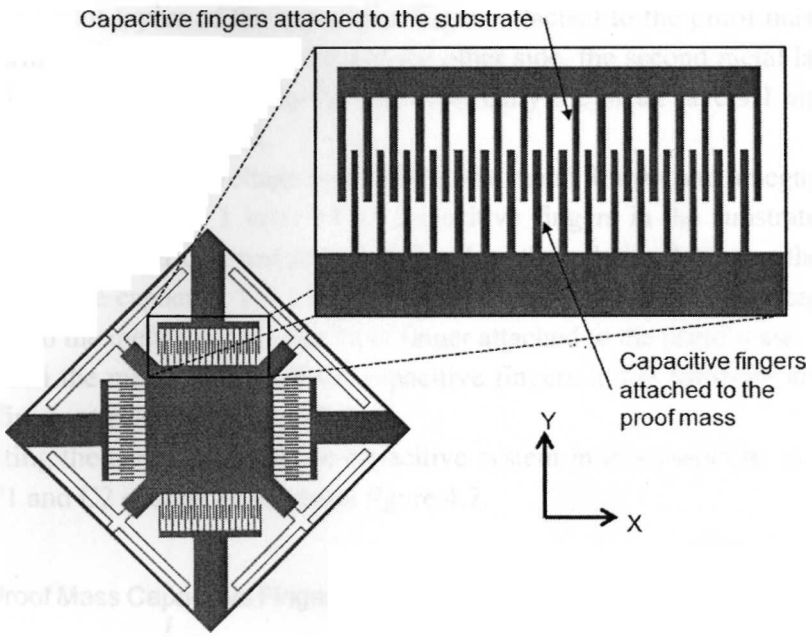

Figure 4.5: Structure of the capacitive system

The CMOS-MEMS accelerometer will measure accelerations in the out-of-plane direction, so the proof mass will be restricted to move only in the Z-axis. To measure these displacements, all three metal layers of the CMOS process will be used to form a capacitive system whose capacitance will change as the capacitive fingers in the proof mass move up or down. Figure 4.6 show the layout of the capacitive fingers used to measure displacements in the Z-axis.

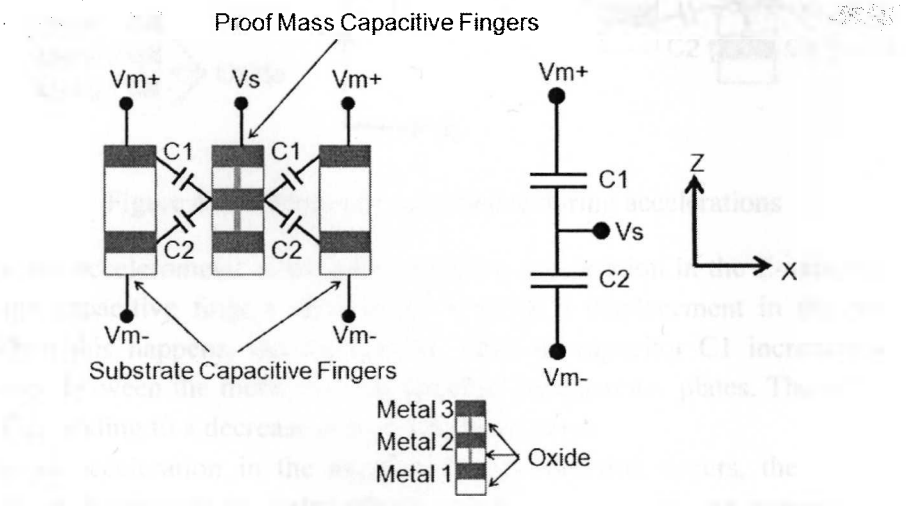

Figure 4.6: Connection scheme of the capacitive system

The three metal layers of the capacitive fingers attached to the proof mass are united by metal vias to form a single electrical node. On the other side, the second metal layer is removed from the capacitive fingers attached to the substrate. Only the metal layers 1 and 3 remain but there is no connection between them.

If a positive modulation voltage is applied to the metal 3 layer and a negative modulation voltage is applied to the metal 1 layer of the capacitive fingers in the substrate, the electrical node Vs will have an electric potential proportional to the relation between the values of the capacitors 1 and 2. The capacitor 1 is formed between the metal 3 layer of the capacitive fingers in the substrate and the metals in the capacitive finger attached to the proof mass. The capacitor 2 is formed between the metal 1 layer of the capacitive fingers in the substrate and the metals in the capacitive finger attached to the proof mass.

Connecting the metal layers of the capacitive system in this particular manner, the value of capacitors C1 and C2 change as shown in figure 4.7.

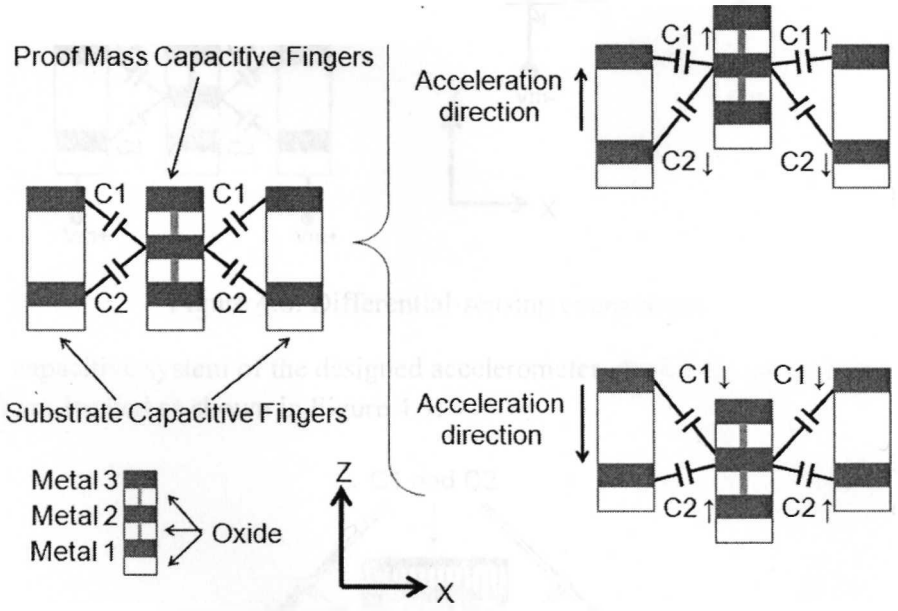

Figure 4.7: Changes in capacitance during accelerations

When the accelerometer undergoes a positive acceleration in the Z-axis, the proof mass along with the capacitive fingers attached to it suffer a displacement in the positive Z-axis direction. When this happens, the capacitance value of capacitor C1 increases as there is a smaller distance between the metal surfaces forming the capacitor plates. The opposite happens to capacitor C2, leading to a decrease in its capacitance value.

When an acceleration in the negative Z-axis direction occurs, the opposite situation occurs, causing a decrease in the value of the capacitance of C1 and an increase in the value of the capacitance of C2.

If half of the capacitive fingers in the capacitive system use this electrical connection arrangement and the other half uses a similar arrangement in which the connections of the positive and negative modulation voltages are inverted, a capacitive system with differential sensing can be achieved.

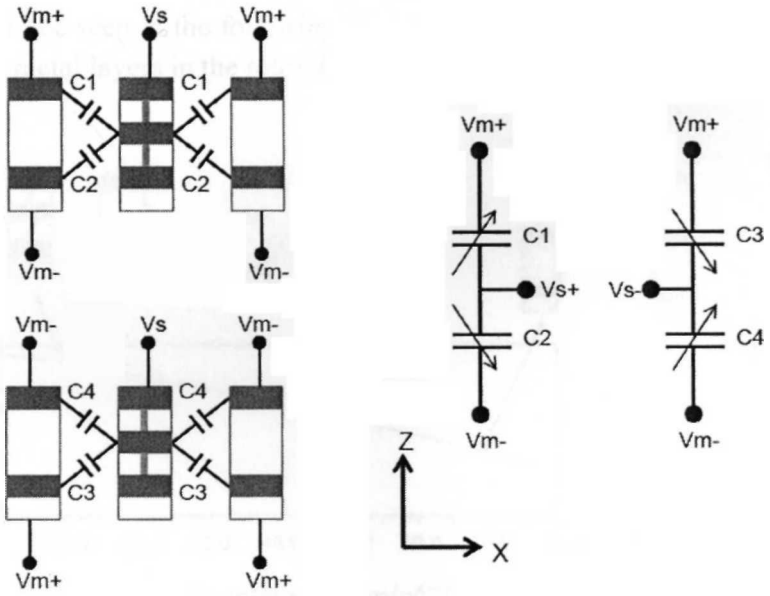

Figure 4.8: Differential-sensing connections

In the capacitive system of the designed accelerometer, the C1-C2 capacitors and the C3 - C4 capacitors are located as shown in Figure 4.9.

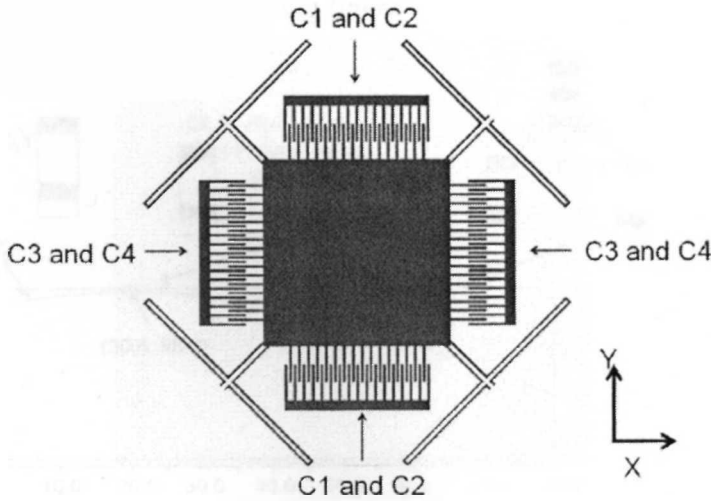

Figure 4.9: Capacitor groups placement

We should consider that the range of accelerations in which the differential measurement of the capacitance can be done is limited. This is because, depending on the acceleration direction, the capacitance between some layers begins to behave in a non-linear manner.

A graph that relates the acceleration undergone by the accelerometer and the capacitance between the capacitive fingers is shown below. When the structure suffers an upward acceleration, it can be seen in the following figure that the capacitance between the M1 layer of the stator and the metal layers in the rotor decreases continuously.

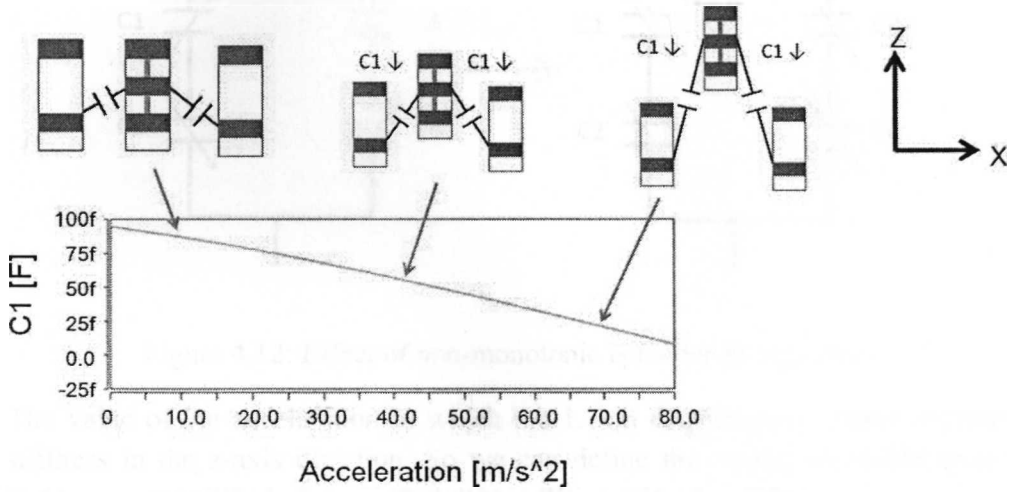

Figure 4.10: Change in capacitance for C1 capacitor upon positive displacement in z-axis

However under the same upward acceleration the capacitance between the M3 layer of the stator and the metal layers of the rotor first increases but after a certain acceleration it starts to decrease, as it can be seen in the following figure.

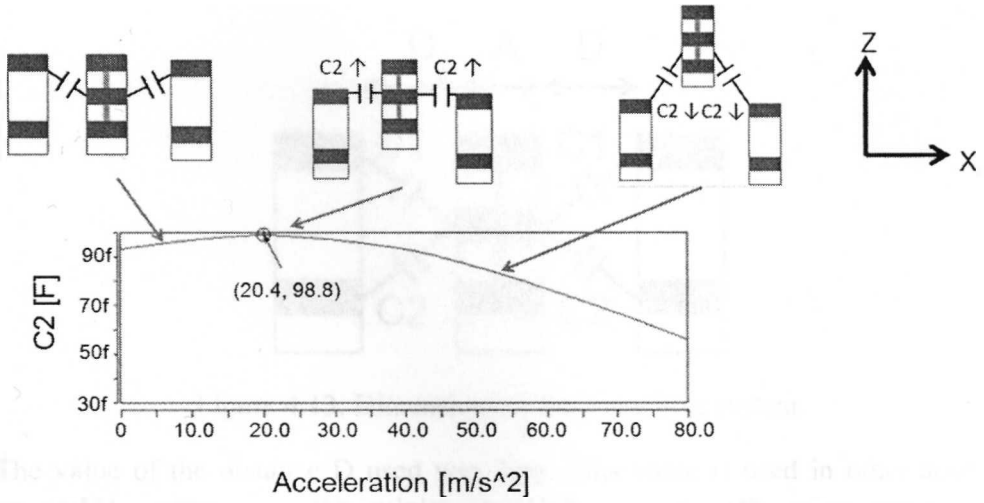

Figure 4.11: Change in capacitance for C2 capacitor upon positive displacement in z-axis

Using the materials and thickness that correspond to the 0.35um CMOS process and the type of capacitive finger structure proposed above, this situation occurs when the central mass suffers a displacement of about 1.7um in the z-axis in either direction. When this happens, the differential capacitive sensing can no longer be made.

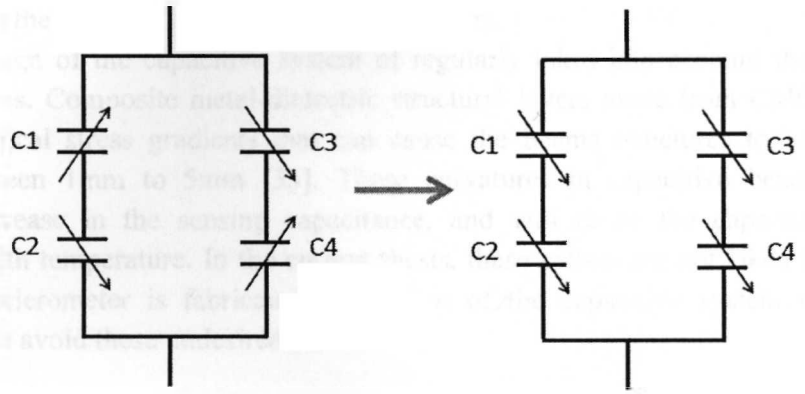

Figure 4.12: Effect of non-monotonic behavior of capacitors

The value of the acceleration in which the 1.7um displacement occurs depends on the spring stiffness in the z-axis direction. So we can define the maximum acceleration that the accelerometer can measure as the one that moves the central mass this particular distance in the z-axis.

The values of the dimensions of the capacitive sensing system were selected to provide the maximum value of capacitance between fingers. This is because having a larger sensing capacitance we can achieve a better sensibility because the effects of parasitic capacitances are diminished.

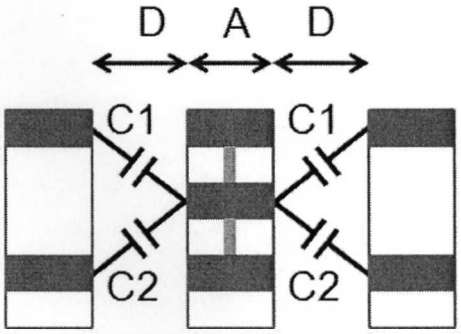

Figure 4.13: Dimensions of the capacitive system

The value of the distance D used was 2um. This value is used in other accelerometer structures and is referred as the minimum value to ensure the post-processing of the accelerometer can be done correctly for similar CMOS processes.

The width A of the rotor capacitive fingers used was 0.9um. This is because several metal vias should be placed inside the rotor finger in order to connect the different metal layers. According to the 0.35um CMOS design rules, a metal via should have a minimum width of 0.5um, and a minimum distance from the end of the metal via to the end of the metal in either metal layer the via is connected to must be 0.2um. The width of the stator capacitive fingers will be held equal to the width of the rotor capacitive fingers.

The design of the capacitive system of regularly takes into account the curling of the capacitive beams. Composite metal-dielectric structural layers made from CMOS interconnect experience vertical stress gradients that can cause the beams structures to have a radius of curvature between 1mm to 5mm [33]. These curvatures in capacitive beams can cause a substantial decrease in the sensing capacitance, and will cause the capacitance to change dramatically with temperature. In the current thesis, these effects are not taken into account, so before the accelerometer is fabricated the design of the capacitive system will need some modifications to avoid these undesired effects.

Chapter 5

Design Space Exploration

In the current chapter the process taken to perform the design space exploration is explained. First the exploration methodology is explained. Afterwards the analytical design exploration is presented. Then the design exploration using computer simulations is explained. Finally the results of both design explorations are compared.

5.1 Exploration Methodology

There are two different approaches to perform the design space exploration of the current MEMS accelerometer. The first one consists in first choosing a generic accelerometer structure and start varying the topology of the structure, evaluating the performance parameters of the accelerometer after each modification is made. The second approach consists in choosing a specific topology and start varying the dimensions of the elements of the accelerometer, evaluating each resulting structure after a specific dimension in changed. This last approach is called a parametric design space exploration. In the current thesis, a parametric design space exploration is performed to 3 different CMOS-MEMS accelerometer topologies to observe the behavior and ranges of the performance characteristics of its structure. The stiffness of the spring system in each axis, the resonance frequencies, the range of accelerations that can be measured, the total area occupied by the mechanical structure of the accelerometer and the cross axis sensitivity of each resulting structure will be evaluated. The basic accelerometer topology that will be used to perform the parametric exploration is shown in figure 5.1.

Specifically, the accelerometer dimensions to be modified correspond to different elements of the spring system. The parametric analysis is done to three different accelerometer topologies. These topologies are similar but the number of spring beams differs between them. The spring system used in the space exploration is be the same as the spring system presented in chapter 4, but the number of short spring beams are 3, 5 and 7.

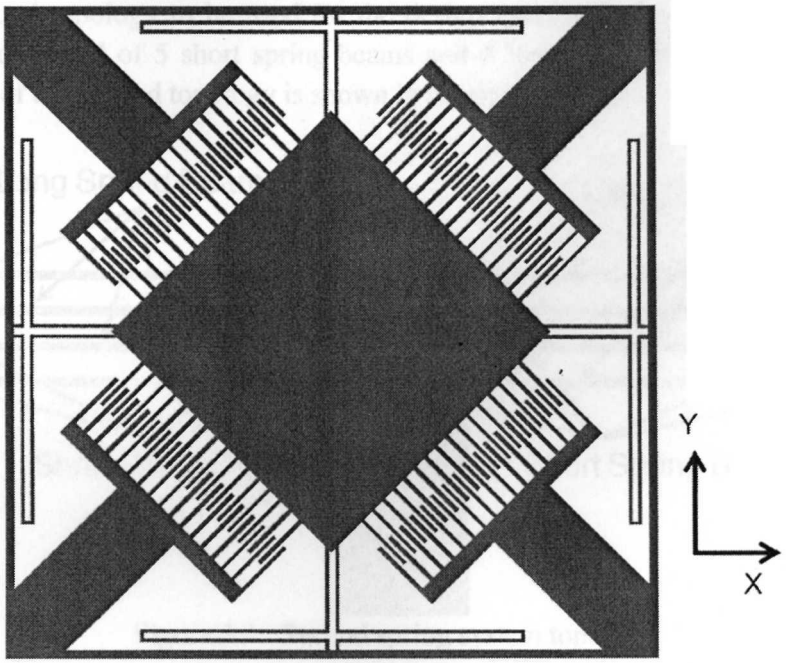

Figure 5.1: CMOS-MEMS accelerometer structure

A segment of two pairs of springs of the first topology, that consists of 3 short spring beams and 2 long spring beams each one, is shown in figure 5.1.

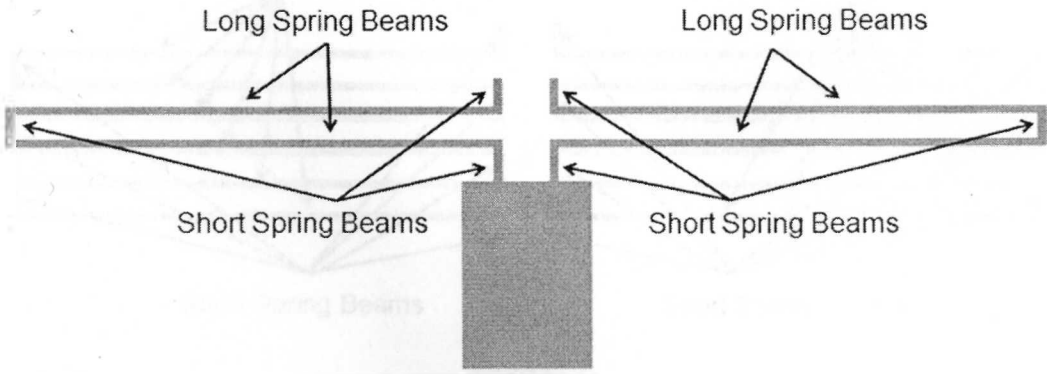

Figure 5.2: First spring system topology

The parameters that will be modified in the exploration will be the length of the long spring beams, the length of the short spring beam and the width of both beams. As mentioned in chapter 4, the thickness of the beams of the spring system will be kept constant and will have a value of 0.865um. The spring system shown above can be modeled using the equations in chapter 4 by giving n the value of 3.

The second topology to be used for the design space exploration uses a similar spring system but is composed of 5 short spring beams and 4 long spring beams. A segment of two pairs of springs of the second topology is shown in figure 5.2.

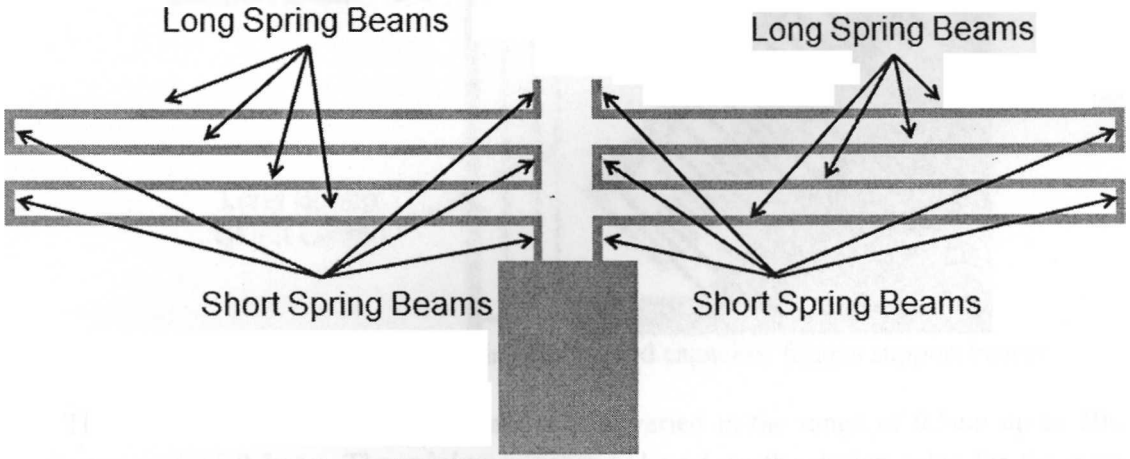

Figure 5.3: Second spring system topology

The third topology is composed of 7 short spring beams and 6 long spring beams in each spring segment. A segment of two pairs of springs of the third topology is shown in figure 5.3.

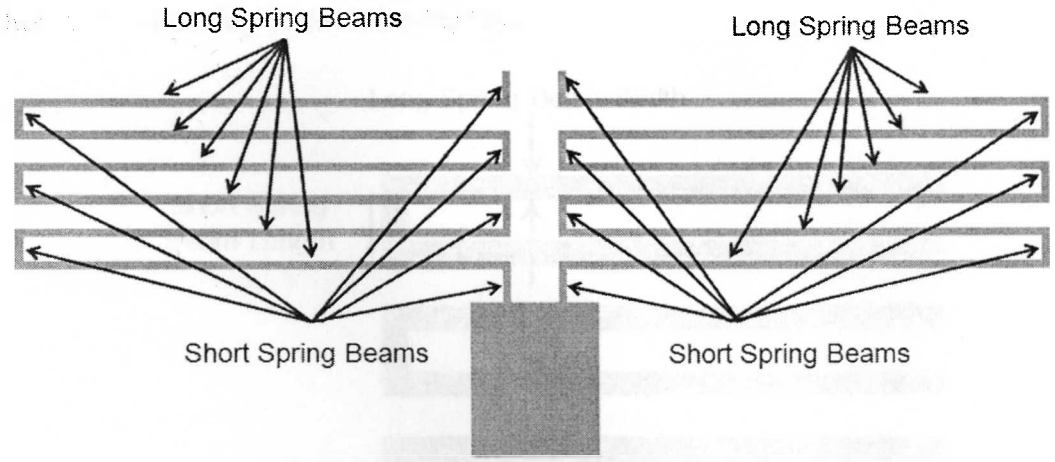

Figure 5.4: Third spring system topology

During the parametric analysis, the length of the long spring beams will be varied in a range of 40 um to 290um, using increments of 5um. The value of 290um was set as an upper limit in order to prevent the spring beams from coming into contact with the structure that supports the capacitive fingers.

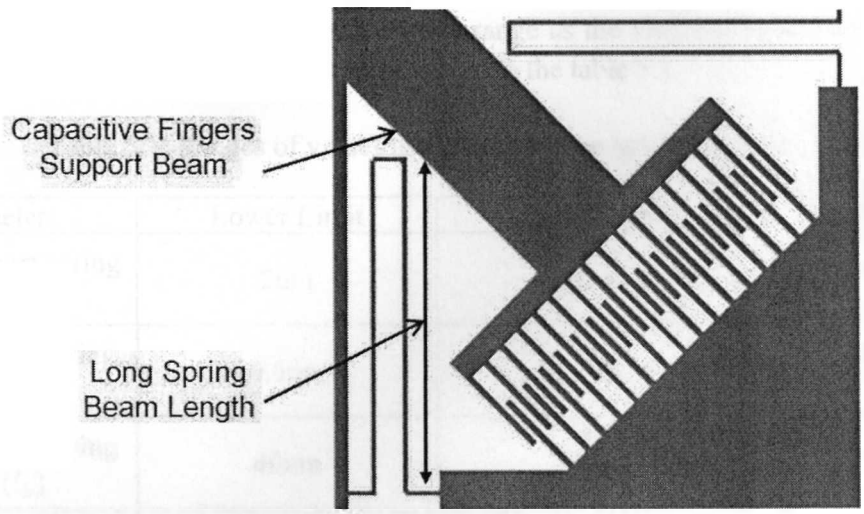

Figure 5.5: Distance between spring beams and capacitor fingers support beams

The width of the long spring beams will be varied in the range of 0.5um up to 20um, using increments of 0.5um. The minimum value is based on the design rules for the current CMOS process in which the minimum width of a metal segment of the metal 1 layer should be equal or larger than 0.5um. The length of the short spring beams will be varied in a range of 2um to 20um, using increments of 1um.

For the particular case of our spring structure, the length of the short beams should be larger than the width of the short beams in order for the pair of long spring beams not to come together, as it can be seen in the following figure.

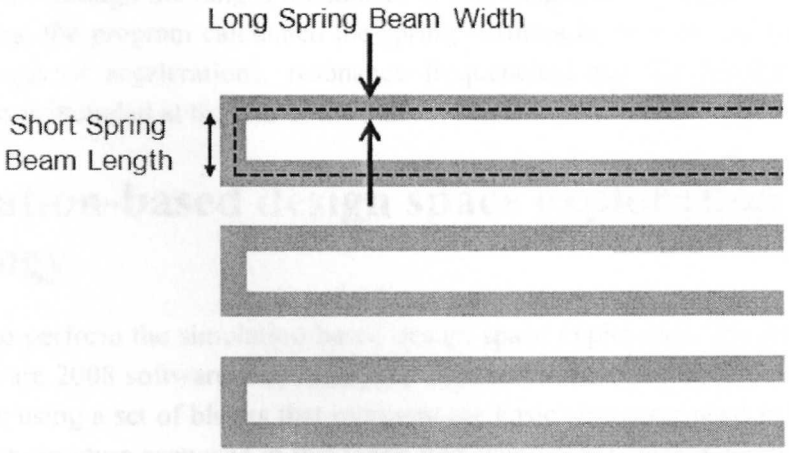

Figure 5.6: Dimensions of the spring system beams

Therefore, the cases in which the length of the short spring beams is shorter than the width of the long beams will not be taken in account for the parametric analysis. The width of

the short spring beams will be varied in the same range as the long spring beams. The design parameters and the values to be used are summarized in the table 5.1.

Table 5.1: Ranges of values used in the design space exploration

Parameter	Lower Limit	Upper Limit	Interval
Length of short spring beam (l_a)	2um	50um	1um
Width of short spring beam (w_a)	0.5um	20um	0.5um
Length of long spring beam (l_b)	40um	290um	5um
Width of long spring beam (w_b)	0.5um	20um	0.5um
Number of short spring beams (n)	3	7	2

5.2 Analytical design space exploration methodology

In order to perform the analytical design space exploration, the formulas presented in chapter 4 are used. Using the Matlab 7.6.0 R2008 software, a program that varied the values for the design variables through the ranges mentioned in this chapter was written [34]. For each set of design variables, the program calculated the spring stiffness in the out-of-plane and in-plane direction, the range of accelerations, resonance frequencies, and the cross-sensitivity. The complete program is included at the end of the current thesis.

5.3 Simulation-based design space exploration methodology

In order to perform the simulation-based design space exploration, the Architect module of the Coventorware 2008 software was used [35]. This software allow us to construct complex MEMS structures using a set of blocks that represent the basic structures used in MEMS design. The accelerometer structure proposed in this thesis was represented using a combination of these blocks, connecting then and configuring their parameters to simulate the mechanical and electrical behavior of the MEMS accelerometer, taking into account the materials of the different layers of the 0.35um CMOS.

Using Architect, each one of the principal components of the MEMS accelerometer, the spring system, the capacitive system and the central mass, were represented using a set of blocks

from the Coventorware software. The schematic representation of these blocks is shown in the following figure.

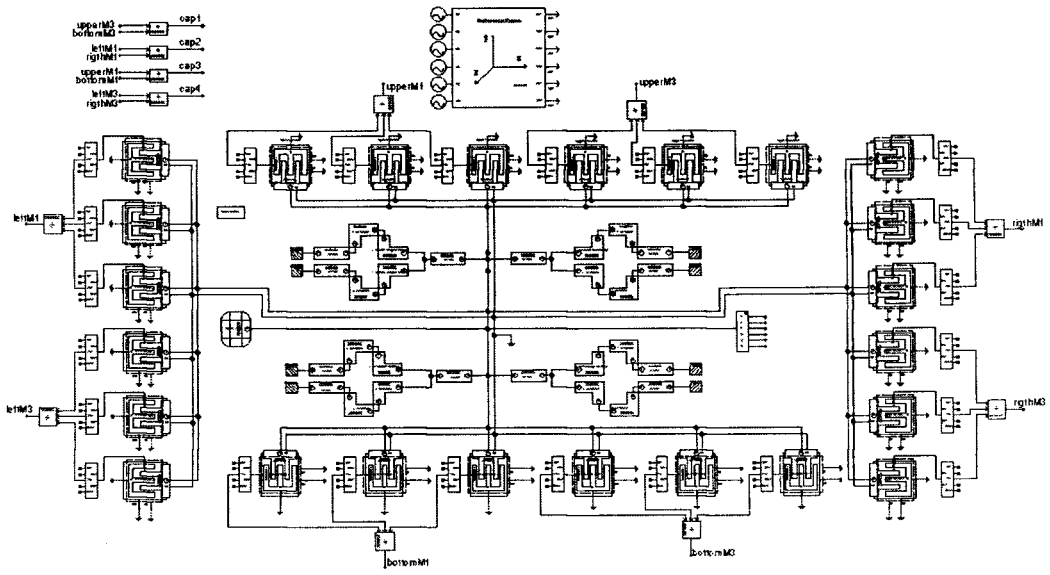

Figure 5.7: CMOS-MEMS accelerometer diagram constructed in Architect

We will now explain about the implementation of the components of the spring system using these building blocks.

5.3.1 Spring System

The spring system was built using a series of blocks that simulate the behavior of spring beams with different shapes, as well as using blocks that represent the union of the spring beams to the silicon substrate. The principal inputs to these blocks are their position relative to the center of the structure, the length, thickness and width of the beam and the layers of materials that form the beam. Because in each one of the spring system designs the number of spring beams is different, each spring system has a different number of building blocks.

The first spring system, which has 3 short spring beams per segment, is modeled using the building blocks shown in figure 5.8. For the rest of the spring system topologies, the blocks are arranged in a similar fashion, only adding the necessary blocks to simulate the extra beams, as shown in figure 5.9 and figure 5.10.

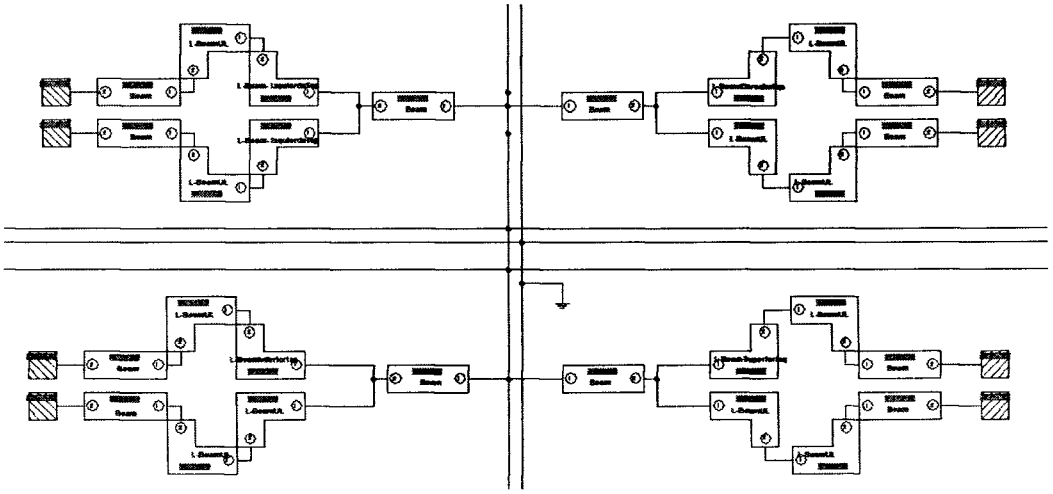

Figure 5.8: Architect schematic of the spring system for topology with parameter n=3

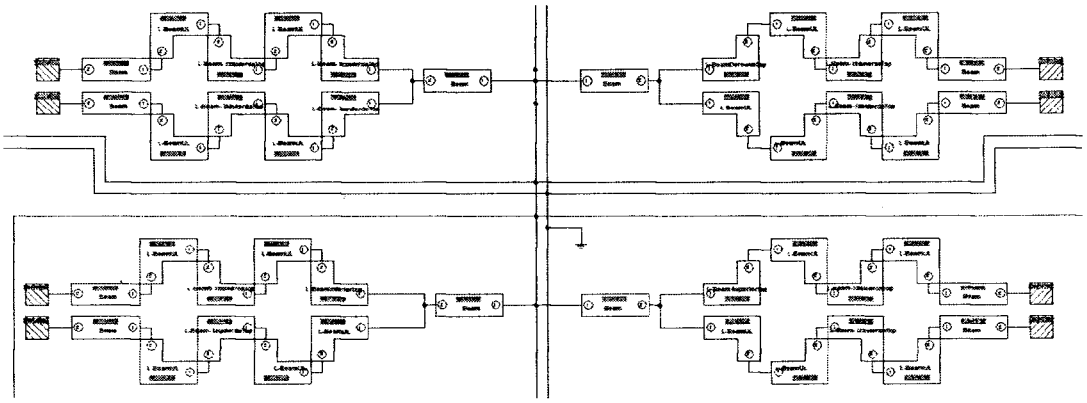

Figure 5.9: Architect schematic of the spring system for topology with parameter n=5

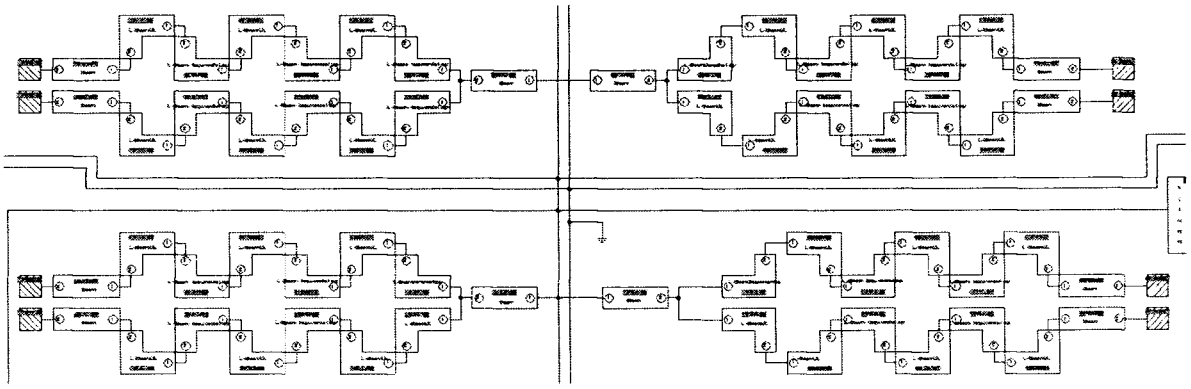

Figure 5.10: Architect schematic of the spring system for topology with parameter n=7

The design parameters are defined as variables within each one of the building blocks. Inside the Architect module, a script in which cycles through the design parameters within the ranges proposed was written. At the end of each cycle, the script simulates the structure and the main characteristics to evaluate the design are saved into a file. In order to obtain the spring stiffness of the system, a small signal analysis is performed to each resulting structure and the resonance frequencies in the x and z axes are obtained. Due to the symmetry of the structure, the resonance frequency in the x and y direction is the same. As in was explained in chapter 3, knowing the value of the mass of the structure and the resonance frequency, the value of the spring constant in a specific direction can be calculated.

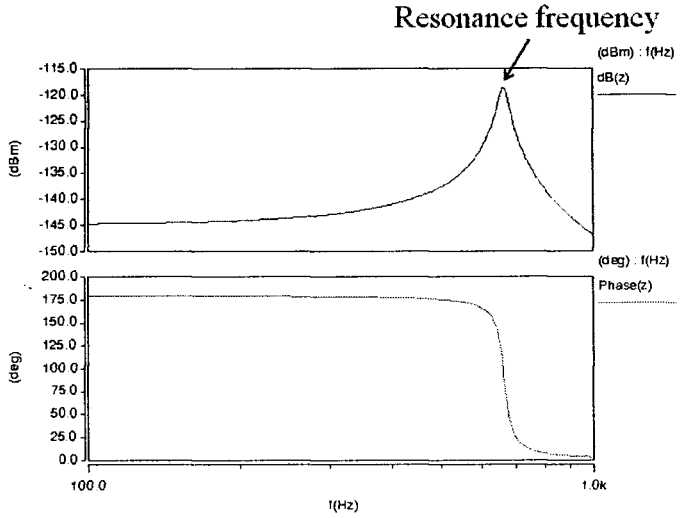

Figure 5.11: Resonance frequency identification in a small signal analysis.

The script found the resonance frequency by identifying the value of the frequency at the point of the maximum amplitude. The range of the accelerations to be measured was obtained using the spring constant in the z-axis direction. As it was mentioned in the previous chapter, the range of accelerations that can be measured before the capacitive measurements stop acting in a linear fashion depend on the spring constant of the spring system .The non-linear behavior of the capacitive system starts when the central mass suffers a displacement of +/- 1.7um from its original position. The range of accelerations with units of g can be calculated by the following formula.

$$range = \frac{k_z * 1.7um}{m * 9.7976\frac{m}{s^2}} \tag{5.1}$$

The total area of the structure can be calculated by knowing the length of the spring beams and the number of short spring beams in the structure, as shown in the following figure.

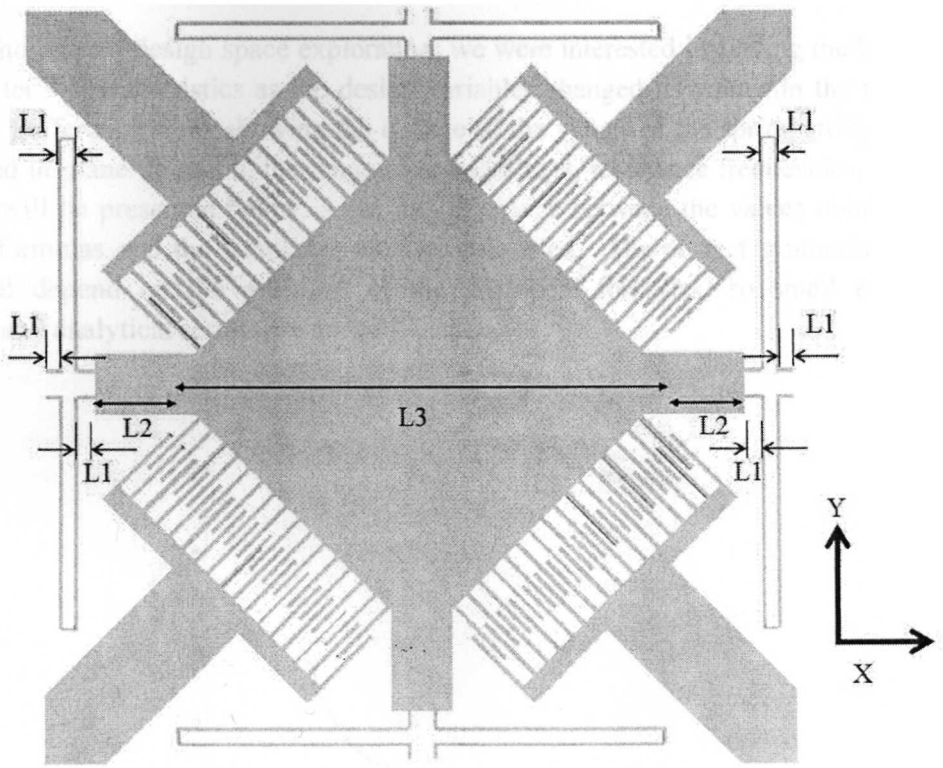

Figure 5.12: Dimensions of the accelerometer structure

L1 represents the length of the short spring beams with variable length, L2 is the length of the lateral supports and L3 depends on the mass dimensions. The dimensions of the mass in this analysis will be fixed to a 400umx400um square mass, so L3 is equal to 566um. The supports will have a fixed width of 120um. So the total area of the accelerometer structure can be calculated as

$$total\ area = (2 * 120um + 565um + n * L1)^2 \tag{5.2}$$

Finally, the cross-axis sensitivity can be calculated after obtaining the spring stiffness in the z-axis and x-axis directions using the following formula.

$$cross\ axis\ sensitivity = \frac{k_z}{k_x} \tag{5.3}$$

5.4 Results of the design space exploration

In the present design space exploration, we were interested in finding the behavior of the accelerometer's characteristics as the design variables changed its values in the ranges defined previously. Different graphs showing the change of the values of the spring stiffness in the out-of-plane and in-plane direction, the range of accelerations, resonance frequencies, and the cross-sensitivity will be presented below. Also, the difference between the values obtained using the analytical formulas and the simulation will be presented. The correct synthesis of the spring system will depend on the accuracy of the analytical formulas, so small errors between simulation and analytical results are desired.

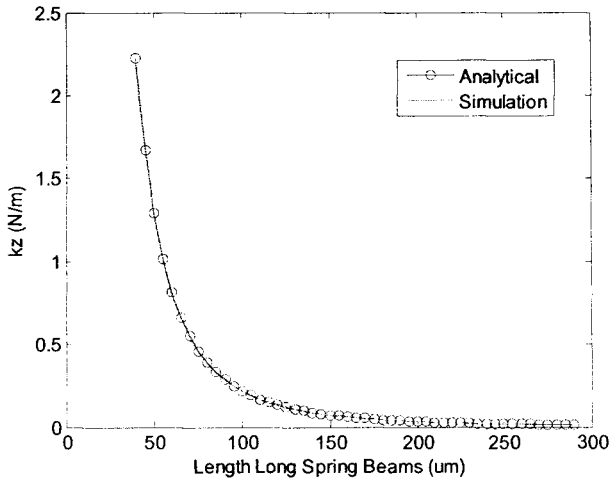

Figure 5.13: Spring system stiffness vs. length of the long spring beams

The first variable to be analyzed is the length of the large spring beams. It will be varied in the range 40um to 290 um with a 5 um interval, leaving the rest of the design variables in their lower limits. The stiffness constant of the spring system in the z-axis direction is calculated for each value of the length of the large spring beams.

For this variable, the maximum error between the simulation and analytical results is 3.91%. The graphs of the resonance frequency and the range of accelerations are shown below. Because the resonance frequency and the maximum range of acceleration are closely related to the spring stiffness in the z-axis, the graphs in figure 5.14 are very similar to the graph in figure 5.13. A maximum error of 1.46% and 4.17% resulted for these cases.

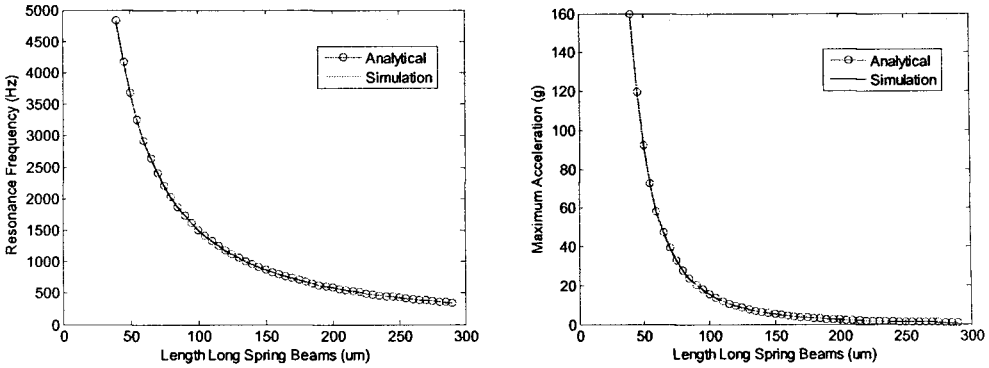

Figure 5.14: Resonance frequency and acceleration range vs. length of the long spring beams

The change in the cross-axis sensitivity, where the length of the long spring beams change is shown below.

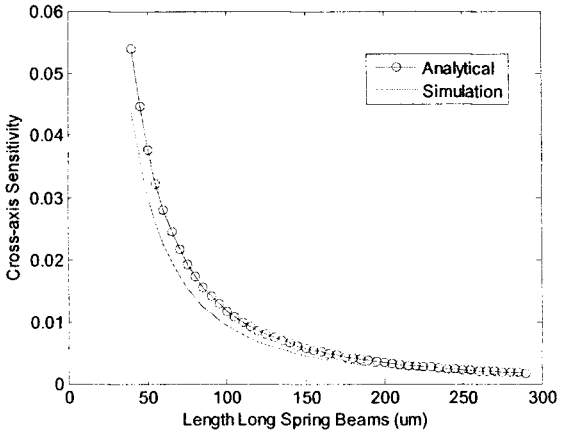

Figure 5.15: Cross-axis sensitivity vs. length of the long spring beams

In the case of the cross-axis sensitivity, a maximum error of 28.09% was found. It was found that the problem behind this error is the calculation of the stiffness constant in the in-plane non compliant direction. However, it was observed that this error was very stable, having errors in the range of 23.66% to 28.09%, so an adjustment to the analytical values can be made to match the simulation values. All of the accelerometers characteristics graphed change monotonically as the length increases. Because the total area does not depend on the length of the long spring beams, the total area of the structure remained constant, with a value of $0.6686mm^2$. From these graphs it can be seen that as the length of the long spring beams increases, the spring stiffness, the frequency range to measure, the maximum acceleration and the cross-axis acceleration tend to diminish.

The second variable to be analyzed is the length of the short spring beams. It will be varied in the range 2um to 50 um with a 0.5 um interval, leaving the rest of the design variables in their lower limits.

The stiffness constant of the spring system in the z-axis direction is calculated for each value of the length of the short spring beams.

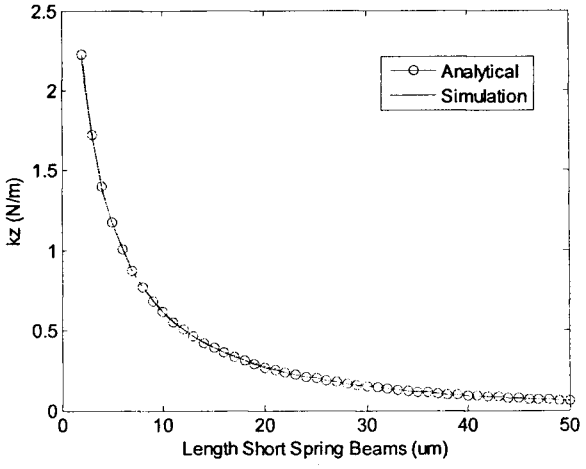

Figure 5.16: Spring system stiffness vs. length of the short spring beams

A maximum error of 1.61% was obtained in this analysis. The graphs of the resonance frequency and the range of accelerations are shown below, for variations in the short spring beam length. A maximum error of 0.76% and 1.63% resulted for these cases, respectively.

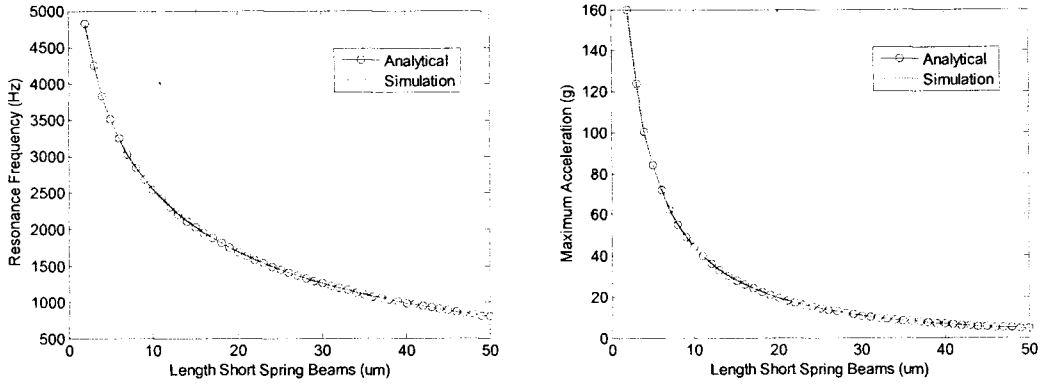

Figure 5.17: Resonance frequency and acceleration range vs. length of the short spring beams

The change in the cross-axis sensitivity, where the length of the short spring beams changes, is shown below.

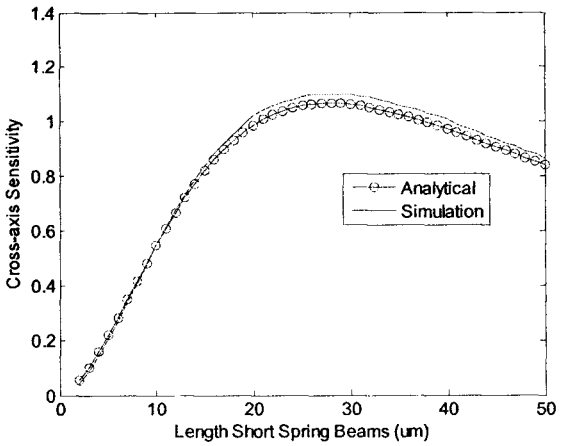

Figure 5.18: Cross axis sensitivity vs. length of the short spring beams

In the case of the cross-axis sensitivity, a maximum error of 24.52% was found. This graph show that the cross-axis sensitivity does not change monotonically with the short spring beam length, as it did with the long spring beam length.

The total area increases linearly with the length of the short spring beams, ranging from $0.6686mm^2$ to $1.2225mm^2$, as shown in figure 5.19.

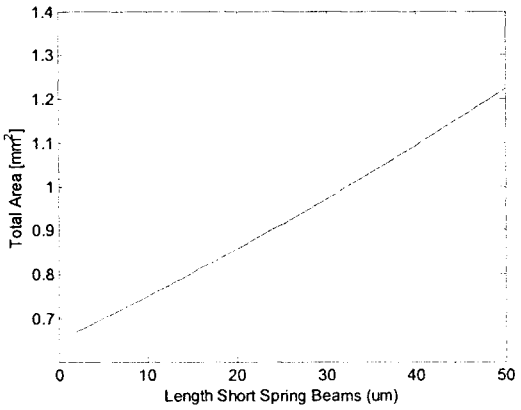

Figure 5.19: Total area vs. length of the short spring beams

From these graphs it can be seen that as the length of the short spring beams increases, the spring stiffness, the frequency range to measure, and the maximum acceleration decreases, while the area increases and the cross-axis acceleration increase until a certain point, and then decreases.

The third variable to be analyzed is the width of the long spring beams. It will be varied in the range 0.5um to 20 um with a 0.5 um interval. The long beams must be less than the length of the short beams in order to avoid the long beams from touching each other. Because of this, in

this analysis the length of the short beams will have a fixed value of 25um, while the other design parameters are held at their minimum values. The stiffness constant of the spring system in the z-axis direction is calculated for each value of the width of the long spring beams.

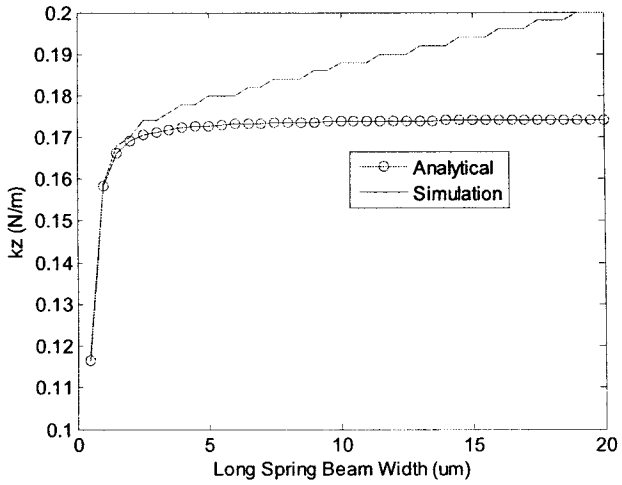

Figure 5.20: Spring stiffness vs. width of the long spring beams

A maximum error of 12% was obtained in this analysis. The graphs of the resonance frequency and the range of accelerations are shown below, for variations in the long spring beam`s width. A maximum error of 6.3% and 13% resulted for these cases, respectively.

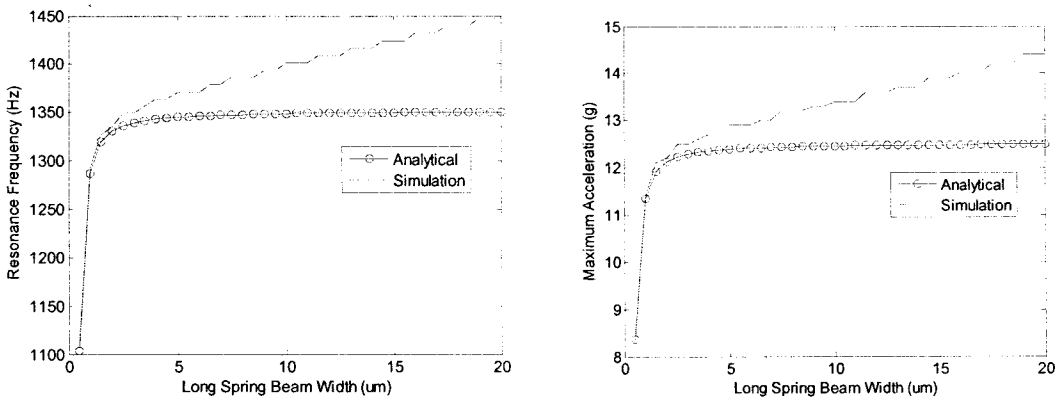

Figure 5.21: Resonance frequency and acceleration range vs. width of long spring beams

The change in the cross-axis sensitivity, where the width of the long spring beams change is shown below.

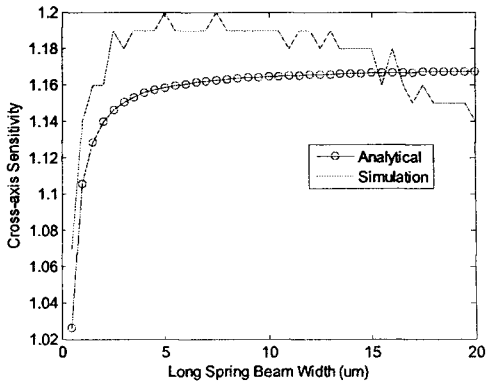

Figure 5.22: Cross-axis sensitivity vs. width of long spring beams

In the case of the cross-axis sensitivity, a maximum error of 4.07% was found. All of the characteristics shown above increase monotonically as the width of the long spring beam increases, except for the cross-axis sensitivity, where the sensitivity suffers an increase as the width increases but it decreases afterwards. However this behavior of the cross-axis sensibility is not seen in the analytical results. It may be seen from the stiffness in the z-axis direction graph that the analytical results for the resonance frequency, spring stiffness and acceleration range increase until they start to converge to a specific value, while the simulation results for these variables continue to increase. This may be due to some mechanical effects not included in the analytical formulation. Because the total area does not depend on the length of the long spring beams, the total area of the structure remained constant, with a value of $0.9133mm^2$.

The fourth variable to be analyzed is the width of the short spring beams. It will be varied in the range 0.5um to 20 um with a 0.5 um interval, leaving the rest of the design variables in their lower limits. The stiffness constant of the spring system in the z-axis direction is calculated for each value of the width of the short spring beams.

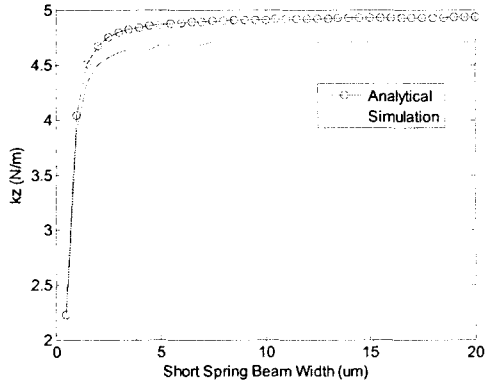

Figure 5.23: Spring stiffness vs. width of the short spring beams

A maximum error of 4.69% was obtained in this analysis. The graphs of the resonance frequency and the range of accelerations are shown below, for variations in the short spring beam width a maximum error of 2.29% and 4.72% resulted for these cases, respectively.

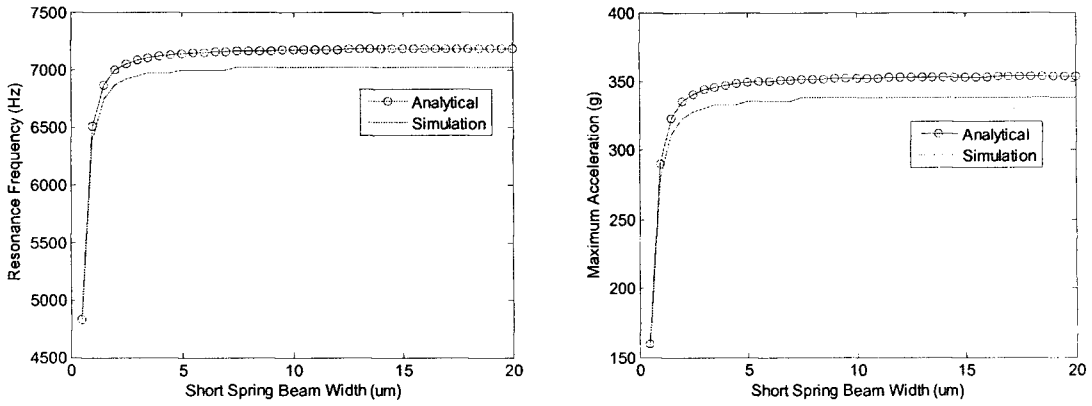

Figure 5.24: Resonance frequency and acceleration range vs. width of the short spring beams

The change in the cross-axis sensitivity, where the width of the short spring beams change is shown below.

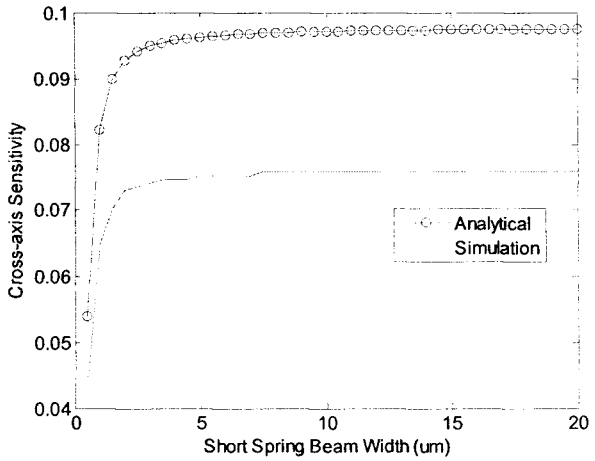

Figure 5.25: Cross-axis sensitivity vs. width of short spring beams

In the case of the cross-axis sensitivity, a maximum error of 20.7% was found. All of the characteristics shown above increase monotonically as the width of the long spring beam increases. It may be seen from the stiffness in the z-axis direction graph that after a width of about 3um, an increase in width no longer affects the stiffness substantially, this may be because the width of the short spring beam is much bigger than the width of the long spring beam and only the long beams act as springs in the z-axis.

Because the total area does not depend on the length of the long spring beams, the total area of the structure remained constant, with a value of $0.6686mm^2$.

Finally, the fifth variable to be analyzed is the number of short spring beams. The number of short spring beams will be varied and will have the values of 3, 5 and 7 beams. In these cases, the number of long spring beams will be 2, 4 and 6 respectively. The rest of the design variables will be left in their lower limits.

The stiffness constant of the spring system in the z-axis direction is calculated for each value of the number of short spring beams.

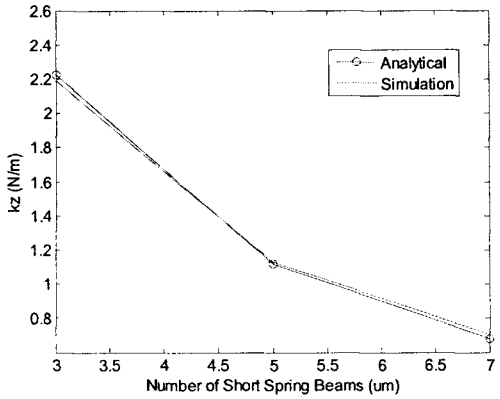

Figure 5.26: Spring stiffness vs. number of short spring beams

A maximum error of 3.51% was obtained in this analysis. The graphs of the resonance frequency and the range of accelerations are shown below, for variations in the number of short spring beams. A maximum error of 1.74% and 3.45% resulted for these cases, respectively.

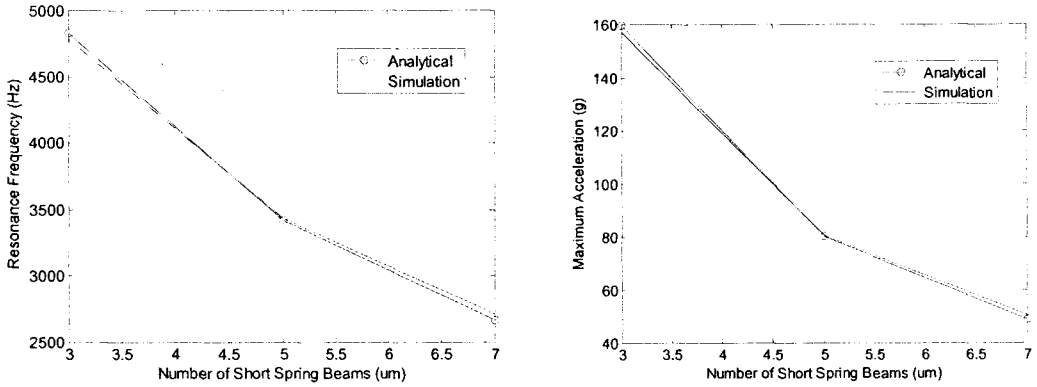

Figure 5.27: Resonance frequency and maximum acceleration vs. number of short spring beams

The change in the cross-axis sensitivity, where the width of the short spring beams change is shown below.

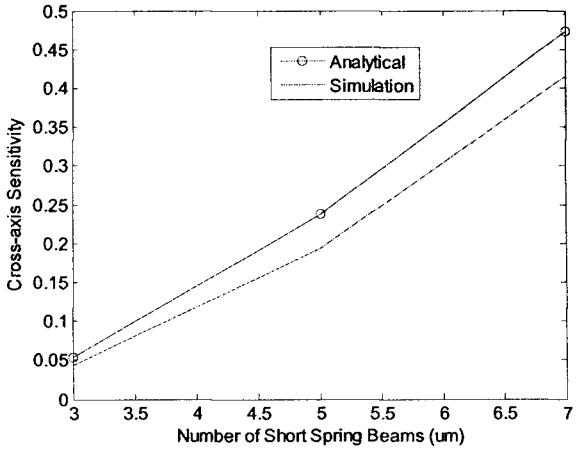

Figure 5.28: Cross-axis sensitivity vs. number of short spring beams

In the case of the cross-axis sensitivity, a maximum error of 24.81% was found. All of the performance values shown above change monotonically as the number of the short spring beams increase. The stiffness in the z-axis direction, the resonance frequency and the maximum acceleration increase, while the cross-axis sensitivity decreases its value. As expected, the total area of the accelerometer also increases as the number of short beams increases, as shown in the figure below.

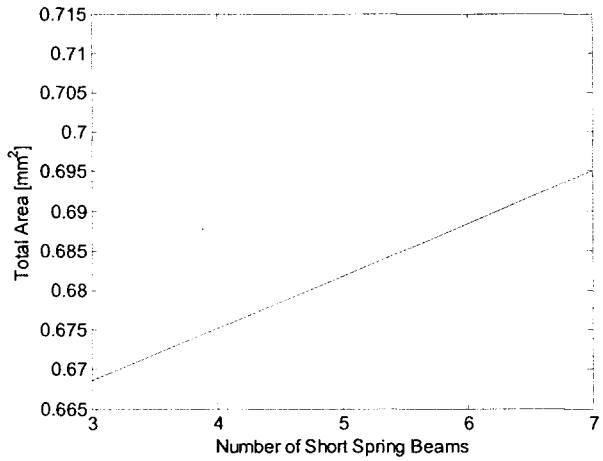

Figure 5.29: Total area vs. number of short spring beams

The change in the characteristics of the spring system of the accelerometer as the design parameters change, taking into account the simulation results, can be summarized in the table below.

Table 5.2 Change in performance parameters

Parameter	Stiffness Z-axis	Resonance Frequency	Maximum Acceleration	Cross-axis Sensitivity	Total Area
Length of long spring beam (l_b)	↓	↓	↓	↓	-
Length of short spring beam (l_a)	↓	↓	↓	Non-monotonic	↑
Width of short spring beam (w_a)	↑	↑	↑	↑	-
Width of long spring beam (w_b)	↑	↑	↑	Non-monotonic	-
Number of short spring beams (n)	↓	↓	↓	↑	↑

Using the information in the table above, the maximum and minimum value that can be achieved with the ranges of the parameter values proposed in table 5.1 are shown below. Because the design parameters affect more than one value simultaneously, some of the minimum or maximum values cannot be achieved simultaneously.

Table 5.3: Maximum and minimum values of performance parameters

	Stiffness Z-axis	Resonance Frequency	Maximum Acceleration	Cross-axis Sensitivity	Total Area
Minimum value	4.14e-4 N/m	66 Hz	0.0297 g	5.8253e-5	0.6588 mm^2
Maximum value	14.62 N/m	12,373 Hz	1048 g	1.16	2.2671 mm^2

Chapter 6

CMOS-MEMS Accelerometer's Spring System Synthesis

In this chapter an approach to the synthesis of a CMOS-MEMS accelerometer is presented. In this synthesis procedure, an accelerometer layout that meets the performance requirements selected by the user is generated.

6.1 Synthesis process flow

The CMOS-MEMS z-axis accelerometer synthesis process is divided in three steps. In the first step, the user selects the performance parameters of the accelerometer to be synthesized. In the second step a program will search for an accelerometer structure that best fits the user specifications. In the third step the user is presented with the performance specifications of the best accelerometer found. The user can then decide to accept the presented accelerometer or perform another search using different specifications. In the fourth step the schematic of the resulting accelerometer is presented in Architect ready to generate the layout of the structure.

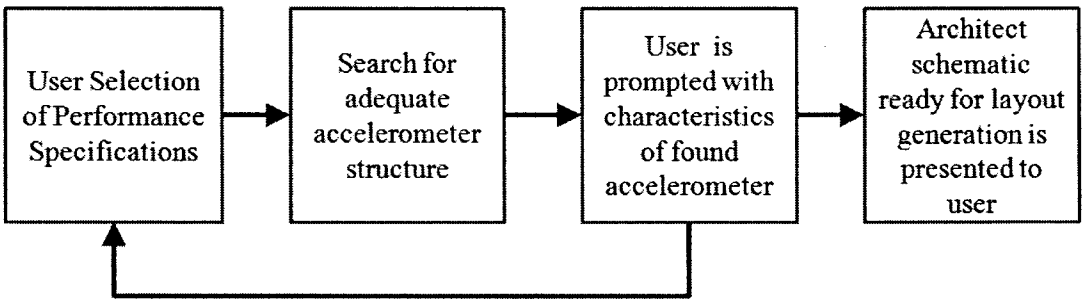

Figure 6.1: Synthesis process flow diagram

In the first step of the synthesis process, the user is presented with a screen were he can select the performance specifications of the accelerometer. In the current synthesis process, the user can select one of three performance specifications to be met, the desired spring system stiffness, the desired resonance frequency or the maximum range of accelerations to be measured.

Additional to one of these specifications, the user can select the desired maximum cross-axis sensitivity and the maximum area of the device.

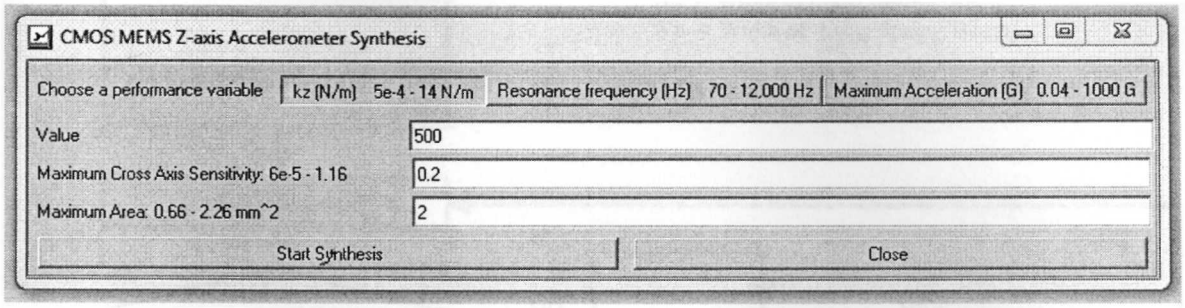

Figure 6.2: User selection of performance specifications

The user is restricted to input a value that should be inside a range of predefined values. These predefined values are taken from the results of the design exploration and shown in table 5.3. After the user selects the desired performance specification and cross-axis sensitivity and maximum area restrictions, an AIM script is run to find the accelerometer that best fits the user specifications.

The code of the script is presented at the end of this thesis in the appendix section. The script basically runs a cycle that modifies the dimensions of the accelerometer, and for each resulting accelerometer structure, its performance characteristics are calculated using the formulas presented in chapter 4. The cycle continues to run until an accelerometer structure that meets the main performance specification with a maximum 1% error margin and at the same time meets the maximum cross-axis sensitivity and the maximum area restrictions. A diagram that explains the search process more in detail is presented in figure 6.4.

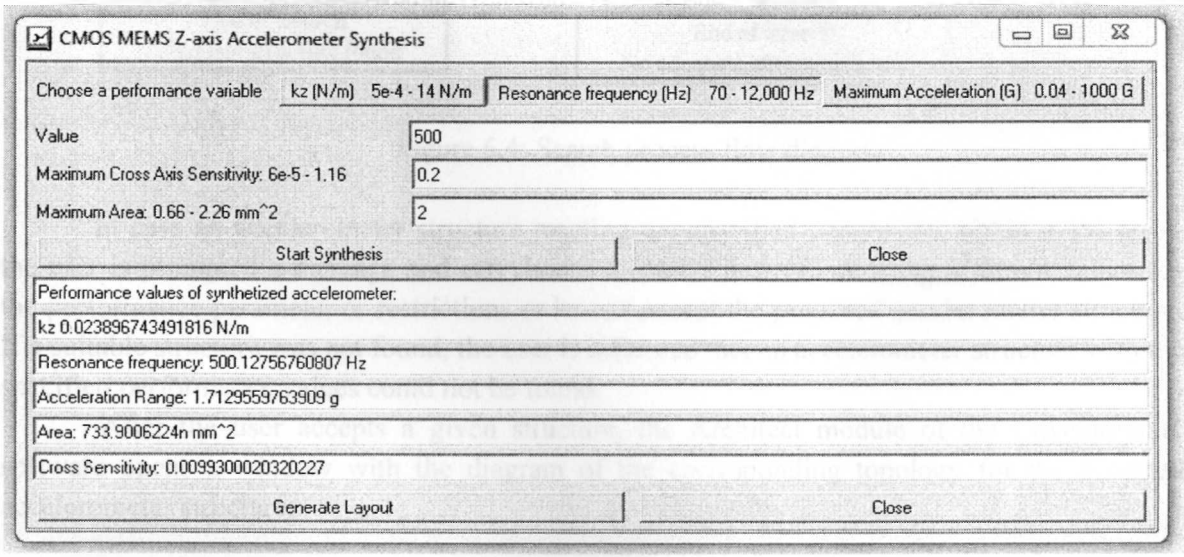

Figure 6.3: Accelerometer structure search results window

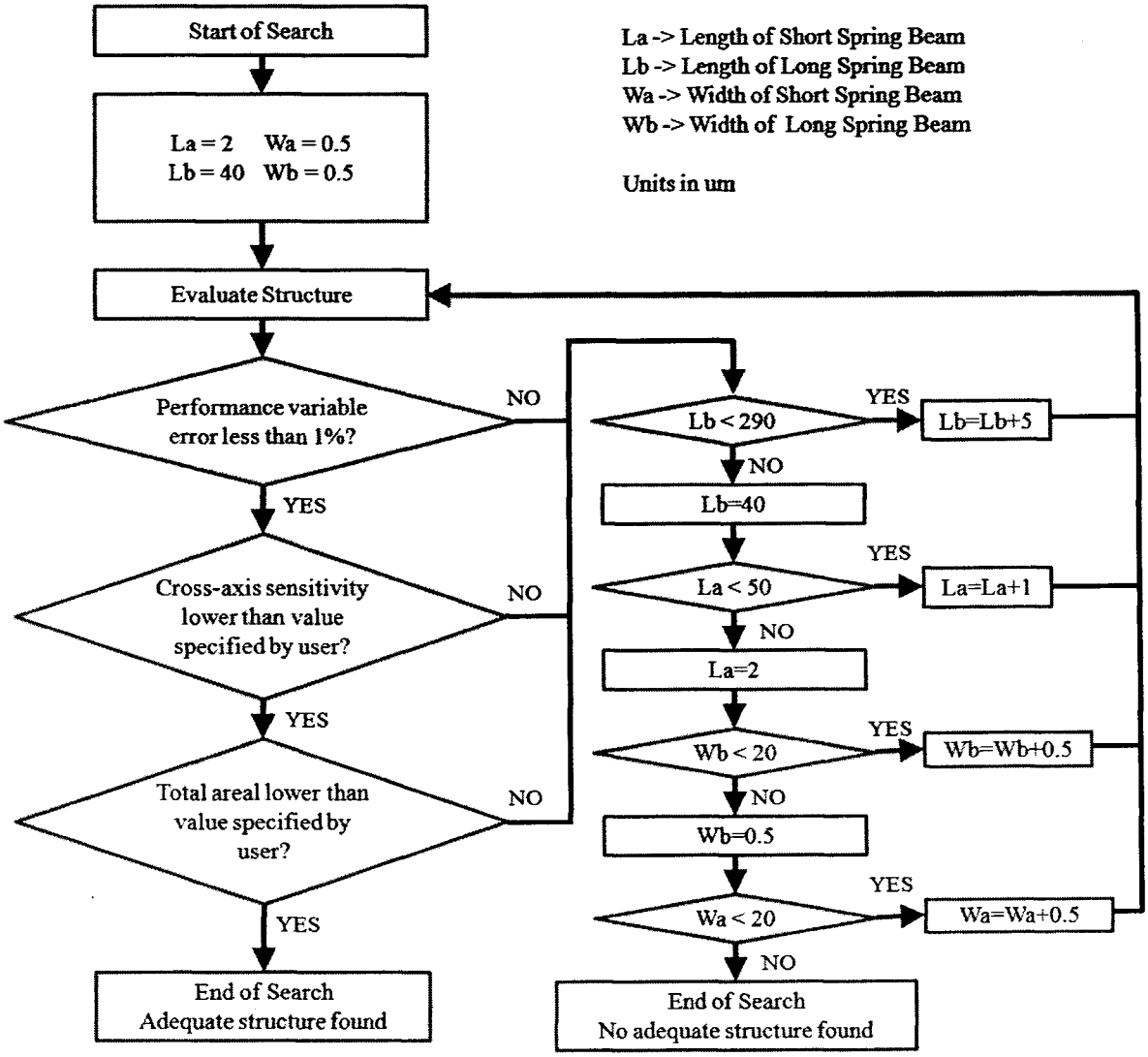

Figure 6.4: Search process flow diagram

In case an accelerometer structure meeting the specified parameters within a 1% error, the user is prompted a message and can choose to start a new search using different values for the performance parameter or restrictions or he can accept the proposed accelerometer structure. If a suitable structure was not found, the user is informed that an accelerometer structure with the specified performance values could not be found.

After the user accepts a given structure, the Architect module of the Coventorware software opens a window with the diagram of the corresponding topology for the accepted accelerometer structure.

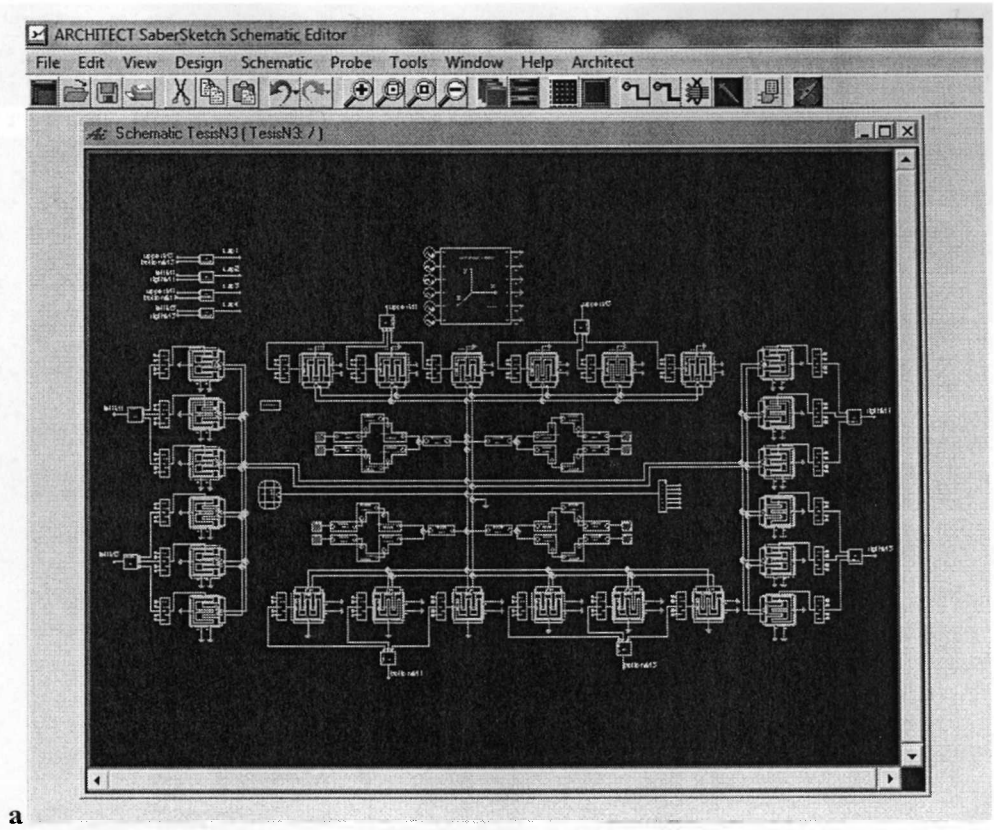

Figure 6.5: Architect diagram of the resulting topology

The user can then instruct Coventorware to generate the layout for the CMOS-MEMS accelerometer. The layout of the accelerometer is generated by the Designer module of the Coventorware software. Because the scripting framework does not allow to allow interaction between the different modules of the Coventorware suite, in the current synthesis program the user needs to export the diagram information manually from the Architect module and then generate and visualize the layout the in the Designed module. The generated layout of the synthesized CMOS-MEMS accelerometer is shown in figure 6.6.

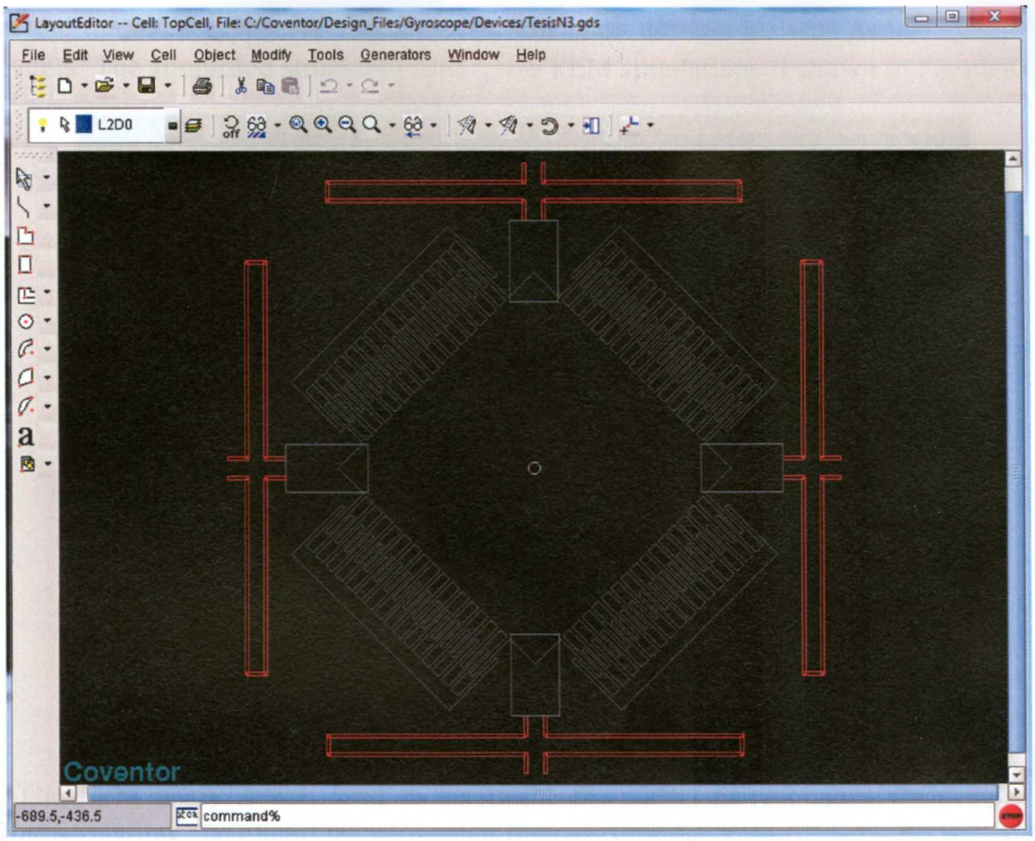

Figure 6.6: Layout of the resulting accelerometer structure

6.2 Evaluation of performance specifications of synthesized accelerometers through FEM analysis

A FEM analysis will be applied to several synthesized accelerometer structures to verify the performance of the synthesis process. An ideal synthesis process should render structures that, when evaluated in a FEM analysis, show performance characteristics that are equal or very similar to the performances characteristics specified by the user.

The results of 5 synthesized structures will be presented in this evaluation. The performance variable selected in the program was the resonance frequency in the z-axis. However, because the program shows the calculated spring stiffness in the z-axis and the acceleration range in the search results window, the values predicted by the synthesis program and the values from the FEM analysis will be able to be compared.

To reduce the time it took for FEM simulations to be completed, the accelerometer structure was modified. These simulations calculate only the mechanical properties of the structure, so the capacitive fingers have no influence in the simulation. Because of this, the capacitive fingers where removed to reduce the FEM mesh complexity. To compensate for the

mass of the removed capacitive fingers, the proof mass dimensions was increased to 436x436 micrometers. The simplified structured used in the FEM simulations is shown in Figure 6.7.

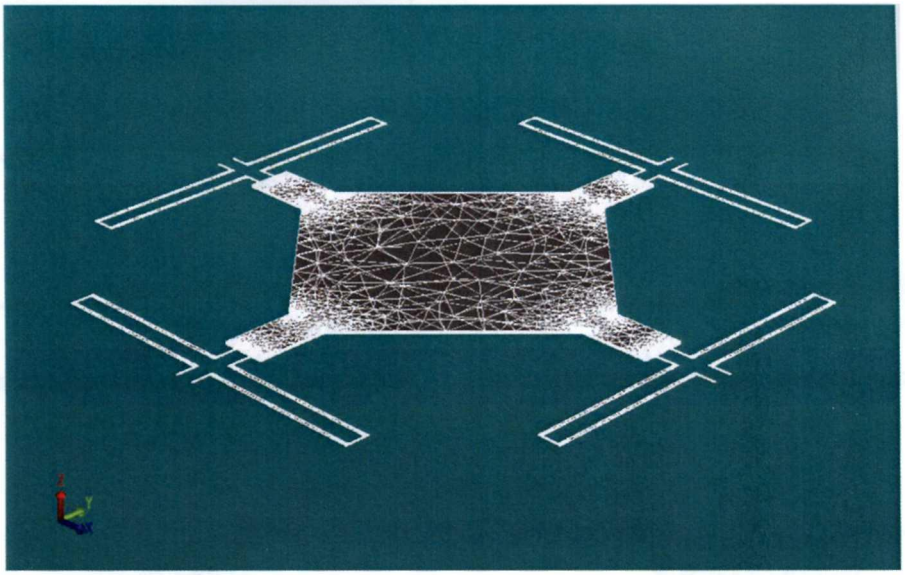

Figure 6.7: Simplified Structure for FEM Simulation

The FEM analysis was used to determine the modal or resonance frequencies of the simplified structures. To obtain the resonance frequency in the X and Z axis, the various modal shapes were analyzed visually and the shapes that corresponded to movements in the X and Z axis where selected. An example of these modes is presented in figure 6.8.

Using these resonance frequencies the spring stiffness, acceleration range and cross-axis sensitivity could also be obtained. In the calculations performed in the synthesis program, the mass is assumed to stay constant, taking only into account the mass of the proof mass, the capacitive fingers and the lateral support beams. However the mass of the spring was not taken into consideration. The Analyzer module of the Coventorware software does take into account the effective spring mass and presents us the total effective mass for each axis as part of the results of the simulations. This total effective mass was used to calculate the spring stiffness for the FEM analysis.

The accuracy of the FEM analysis results depend in the complexity of the mesh generated for the structure. A more complex mesh generally will render more accurate results. The Designer module of the Coventorware software defines 4 levels of mesh refinement, a higher level giving a more detailed mesh. The FEM simulations used for the evaluation were done with a level 3 mesh complexity, due to hardware limitations.

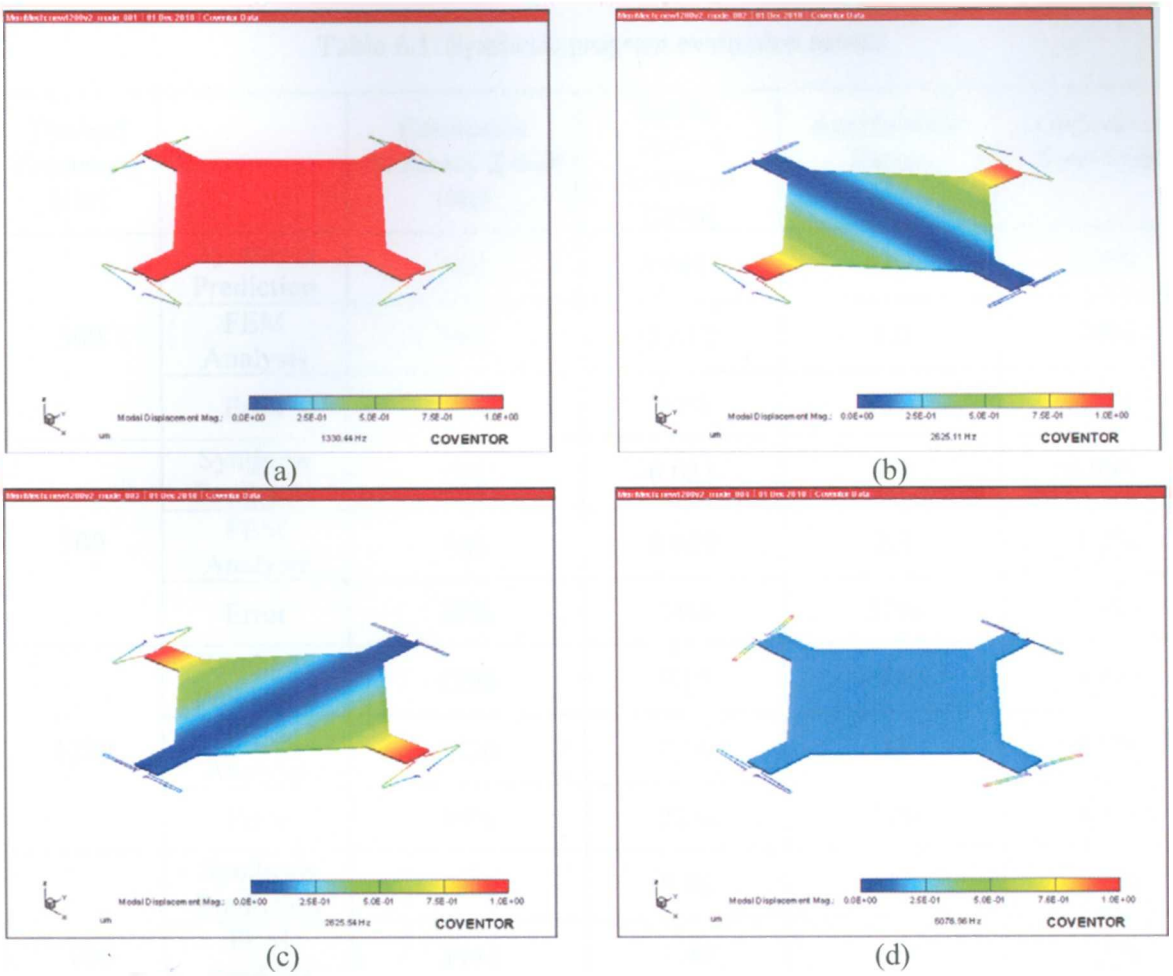

(a) (b) (c) (d)

Figure 6.8: First four resonating modes for the 1200Hz resonance frequency accelerometer (a) First mode at 1330 Hz (Z-axis) (b) Second mode at 2625 Hz (c) Third mode at 2625 Hz (d) Fourth mode at 6076 Hz (Y-axis).

The parameters of these 5 evaluations are summarized in table 6.1. The errors of the performance characteristics varied significantly in each synthesized structure. A maximum error of 31% was obtained when predicting the resonance frequency in the z-axis. For the case of the stiffness in the Z-axis and the acceleration range the maximum errors obtained where significantly higher, 78% and 90% respectively. For the case of the cross-axis sensitivity a maximum error of 21% was obtained.

It was observed that in all the cases, the accelerometer structures had a higher spring stiffness than the one calculated analytically in the synthesis program. In the case the designer knows the accelerometer will be measuring certain accelerations below a determined frequency X and synthesizes an accelerometer with a resonance frequency X, the resonance frequency of the resulting structure will be higher than X and there will be no danger that structure starts resonating. However, the higher spring stiffness will result in less sensitive structures.

Table 6.1: Synthesis program evaluation results

Desired Frequency [Hz]		Resonance frequency Z-axis [Hz]	Spring System Stiffness [N/m]	Acceleration Range [g]	Cross-axis Sensitivity
300	Synthesis Prediction	302	0.0087	0.62	8.7%
	FEM Analysis	365	0.012	1.0	10%
	Error	20%	46%	60%	19%
500	Synthesis Prediction	501	0.023	1.7	0.99%
	FEM Analysis	558	0.029	2.3	1.1%
	Error	11%	24%	37%	16%
1200	Synthesis Prediction	1206	0.13	9.9	4.4%
	FEM Analysis	1330	0.16	13	4.7%
	Error	10%	22%	34%	8.1%
3000	Synthesis Prediction	3002	0.86	61.7	2.3%
	FEM Analysis	3944	1.49	117	2.5%
	Error	31%	78%	90%	9.9%
5000	Synthesis Prediction	5007	2.3	171	1%
	FEM Analysis	5337	2.7	215	0.82%
	Error	6.5%	13%	25%	21%

Chapter 7

Conclusions and Future Work

A design space exploration system of a Z-axis CMOS-MEMS accelerometer and a program for the synthesis of the spring system of this accelerometer were presented.

The design process for this accelerometer and the equations used to model the structure were presented. A particular generic structure was chosen because of the low stiffness value in the z-axis and high stiffness values in the X and Y axis that could be attained, resulting in very small cross-axis sensitivity. In the literature, reported Z-axis accelerometers had cross-axis sensitivity values ranging from 1 to 30%. For the case of the accelerometer layout of the current thesis, even though some groups of dimensions rendered structures with cross-axis sensitivities of up to 116%, most of the structures had a sensitivity of 10% or less. So it is believed that the generic structure layout of the accelerometer was adequately chosen.

The design space exploration showed that structures with performance parameters similar to the performance parameters of reported Z-axis accelerometers listed in table 2.1 could be generated using the selected generic accelerometer layout. Table 2.1 listed accelerometers with resonance frequencies in the z-axis in the range 0.1 to 9.65 kHz, while the generic structure can be modified to have resonance frequencies in the range of 66Hz to 12.3 kHz. This design exploration showed that the analytical model can render results very similar to the results obtained using system-level simulations, with the exception of the case in were the long spring beams thickness was relatively large as shown in figure 5.21. However the maximum error obtained between the analytical and the system-level simulation results for the resonance frequency in the z-axis was 6.3%, a relatively low value. This design space exploration was done to a single accelerometer spring system topology, so it would be interesting to perform a similar exploration using several other spring system topologies and compare the results. It is clear that resonance frequencies below 66 Hz and above 12.3 kHz can be attained using some other different spring system. Additionally, spring systems with resonance frequencies in the range of 66Hz-12.3 kHz with better cross axis sensitivity or less area than the spring system used in this thesis could be found. The synthesis process could then perform a parametric search not only on a single topology but in various topologies to find the most adequate CMOS-MEMS accelerometer topology, meeting the performance parameter and having the least surface area and cross-axis sensitivity. Another enhancement to the synthesis program, although much more complex to realize, might be to perform a search that varied not only dimensions of a determined

topology, but that could also make slight modifications to the shape of the structure of the accelerometer, evaluating the new shape and dimensions of each structure in each iteration of the synthesis program.

The synthesis program developed in the current thesis is intended to constitute a module of a more complex program that would synthesize a CMOS-MEMS accelerometer in a more complete manner. In this synthesis program, to find a structure that met the user performance requirement and limitations, a deep first search algorithm was implemented. This algorithm iterated over the different variables in the specified ranges and evaluated each resulting structure, until a suitable structure was found. The program worked adequately and found accelerometer structures with characteristics very similar to the user specifications. However, it is clear that in the worst case, given that a structure satisfying the user requirements exist, a maximum number of 11,760,000 iterations would have to be done to find the solution (49 possible values for the length of the short spring beam, 40 possible values for the width of both the short and long spring beams, 50 different values for the length of the long beam and 3 different number of short beams). Further work could be done in finding a suitable search algorithm to reduce the search time. The information about the change in the performance parameters when the spring system beam dimensions change could be used to develop a more intelligent search algorithm in the future. A search algorithm such as simulated annealing or a more simple hill climbing algorithm could be developed to bring faster searches and shorter synthesis times.

In the current thesis, to test the accuracy of the model and the formulas used to evaluate each structure, the analytical results were compared with the results of a FEM analysis. During the design space exploration, analytical model showed relatively low errors when compared with macro-model simulations. When evaluating the analytical results with the FEM simulation results, the prediction of the performance values had a much larger errors, up to 31%, when predicting the resonance frequency in the z-axis. Some of the possible causes that could be causing these errors when comparing the analytical results with the FEM simulations are the fact that the effective mass of the spring was not taken into account in the analytical calculations and the lack of complexity of the generated mesh. It must also be considered that the equations of the analytical model do not fully represent the actual structure, and an error will always exist. During the design space exploration, it was found that the analytical model did not correctly model the performance parameters as the width of the long spring beams increased, as shown in figures 5.20 and 5.21. However future work might consider modifying the formulas used so that better predictions of the performance values can be done. As mentioned in section 4.2, some undesired effects such as curling of the capacitive beams where not taken into account for the design of the capacitive system. Curling also affects the performance of the spring system when long beams are used, so future work might involve modifying the design of the beams to reduce these effects.

After some subsequent modifications, the current synthesis method will be able to synthesize much more accurate spring systems structures. However, the spring system is only one of the many systems that compose the CMOS-MEMS accelerometer. In the current synthesis method, the capacitive system of the accelerometer was not modified, neither its topology nor the

dimensions of its structures. The topology and the dimensions of the capacitive system could be modified to find an adequate relation between surface area of the structure and the total sensing capacitance. Having more and bigger capacitive fingers results in higher sensing capacitance, that allows smaller accelerations to be detected as the sensing capacitance is bigger than the inherent parasitic capacitance. However, more and bigger capacitive fingers also occupy a larger area. A synthesis program for the capacitive system might ask the user for the minimum detectable acceleration as a parameter and then calculate the necessary characteristics of the capacitive system. A CMOS-MEMS accelerometer also needs some interface circuitry to demodulate the voltage signal from the accelerometer and amplify the voltage signal. A synthesis method that includes the synthesis of the interface circuitry might prompt the user for the necessary sensibility in volts per unit of acceleration, and perform the layout of a circuit with the necessary signal gain value. In the future, once the synthesis of the spring system, capacitive system and the interface circuitry can be implemented, the synthesis program will be ready to provide the layout of a fully functional CMOS-MEMS accelerometer structure, ready to be fabricated.

Bibliography

[1] S. Wasson, "Intel's Core i3 and i5 dual-core processors", The Tech Report. 04 January 2010. Web. 10 Nov. 2010. <http://techreport.com/articles.x/18216>

[2] F. Faggin, "4004 Microprocessor Display at New Intel Museum (1992)", The Intel 4004. Web. 10 Nov. 2010. <http://www.intel4004.com/museum_display.htm>

[3] "Apple - Iphone4 - Size, weight, battery life, and other specs", Apple Inc. Web. 10 Nov. 2010. <http://www.apple.com/iphone/specs.html>

[4] R. A Polin, and R. Kennett. "Use of monoclonal antibodies in an enzyme immunoassay for rapid identification of group B Streptococcus types II and III", *Journal of Clinical Microbiology*, vol. 11, no.4, Apr. 1980.

[5] "PocketCPR - Your CPR Couach : FAQ". ZOLL Medical Corporation. Web. 10 Nov. 2010. <http://www.pocketcpr.com/faq.html>

[6] J. Warren, "Medtronic Announces Clinical Trial for Breakthrough Technology in Neurostrimulation Therapy for Intractable Chronic Pain", Medtronic. 06 May 2010. Web. 10 Nov. 2010. <http://wwwp.medtronic.com/Newsroom/NewsReleaseDetails.do?itemId=1273149071195>

[7] T. Mukherjee, S. Iyer, G.K. Fedder, "Optimization-based synthesis of microresonators", *Sensors and Actuators A: Physical*, vol. 70, pp. 118-127, Oct. 1998.

[8] T. Mukherjee, Y. Zhou, G.K. Fedder, "Automated optimal synthesis of microaccelerometers", *Twelfth IEEE International Conference on Micro Electro Mechanical Systems, 1999. MEMS '99*, pp.326-331, Jan. 1999.

[9] V. Gupta, 2000. "Approaches to Synthesis of a CMOS Accelerometer". Master's thesis, Carnegie Mellon University.

[10] M.I. Younis, E.M. Abdel-Rahman, A. Nayfeh, "A reduced-order model for electrically actuated microbeam-based MEMS", *Journal of Microelectromechanical Systems*, vol.12, no.5, pp. 672- 680, Oct. 2003.

[11] R. Kamalian, A.M. Agogino, H. Takagi, "Interactive Evolutionary CAD System for MEMS Layout Synthesis", *IEEE International Conference on Systems, Man and Cybernetics, 2006. SMC '06*, vol.4, pp.3469-3474, Oct. 2006.

[12] H. Yang, J. Chengyu, Y. Kai-Leung, X. Yan, Y. Weizheng, "Rapid synthesis of MEMS devices based on element model library and metamodel", *2010 5th IEEE International Conference on Nano/Micro Engineered and Molecular Systems (NEMS)*, pp.301-305, Jan. 2010.

[13] N.R. Lo, E.C. Berg, S.R. Quakkelaar, J.N. Simon, M. Tachiki, L. Hee-Jung, K.S.J. Pister, "Parameterized layout synthesis, extraction, and SPICE simulation for MEMS", *IEEE International Symposium on Circuits and Systems, 1996*, vol.4, pp.481-484, May 1996.

[14] T.D. Tran, M.D. Nguyen, L.T. Nguyen, T.H. Huynh, T.P. Nguyen, "Novel synthesis design of a 3-DOF silicon piezoresistive micro accelerometer", *NEMS 2009. 4th IEEE International Conference on Nano/Micro Engineered and Molecular Systems*, pp.112-115, Jan. 2009.

[15] L.M. Roylance, J.B. Angell, "A batch-fabricated silicon accelerometer", *IEEE Transactions on Electron Devices*, vol.26, no.12, pp. 1911- 1917, Dec 1979

[16] C.C. Hindrichsen, J. Larsen, E.V. Thomsen, K. Hansen, R. Lou-Moller, "Circular piezoelectric accelerometer for high band width application", *Sensors, 2009 IEEE*, pp.475-478, Oct. 2009.

[17] M. Haris, Q. Hongwei, "A CMOS-MEMS piezoresistive accelerometer with large proof mass", *2010 5th IEEE International Conference on Nano/Micro Engineered and Molecular Systems (NEMS)*, pp.309-312, Jan. 2010.

[18] D. Haifeng, H. Yilong, S. Sanmin, H. Lin, L. Jungang, "A novel out-of-plane MEMS tunneling accelerometer with excellent low frequency resolution", *NEMS '06. 1st IEEE International Conference on Nano/Micro Engineered and Molecular Systems, 2006*, pp.821-825, Jan. 2006.

[19] H. Luo, G.K. Fedder, L.R. Carley, "A 1 mG lateral CMOS-MEMS accelerometer", *MEMS 2000. The Thirteenth Annual International Conference on Micro Electro Mechanical Systems, 2000*, pp.502-507, Jan 2000.

[20] Q. Hongwei, F. Deyou, X. Huikai, "An integrated fully-differential CMOS-MEMS z-axis accelerometer utilizing a torsional suspension", *NEMS 2008. 3rd IEEE International Conference on Nano/Micro Engineered and Molecular Systems*, pp.1063-1066, Jan. 2008.

[21] W. Jiangfeng, G.K. Fedder, L.R. Carley, "A low-noise low-offset capacitive sensing amplifier for a 50-μg/vHz monolithic CMOS-MEMS accelerometer", *IEEE Journal of Solid-State Circuits*, vol.39, no.5, pp. 722- 730, May 2004.

[22] L.S. Pakula, H. Yang, P.J. French, "3-D silicon carbide surface micromachined accelerometer compatible with CMOS processing", *ASDAM 2008. International Conference on Advanced Semiconductor Devices and Microsystems*, pp.227-230, Oct. 2008.

[23] Q. Hongwei, F. Deyou, X. Huikai, "A Monolithic CMOS-MEMS 3-Axis Accelerometer With a Low-Noise, Low-Power Dual-Chopper Amplifier", *IEEE Sensors Journal*, vol. 8, no. 9, Sep. 2008.

[24] M.A. Lemkin, B.E. Boser, D. Auslander, J.H. Smith, "A 3-axis force balanced accelerometer using a single proof-mass", *International Conference on Solid State Sensors and Actuators, 1997. TRANSDUCERS '97*, vol.2, pp.1185-1188, Jun. 1997.

[25] T. Ming-Han, S. Chih-Ming, W. Chuanwei, L. Joung, F. Weileun, "A monolithic 3D fully-differential CMOS accelerometer", *NEMS 2008. 3rd IEEE International Conference on Nano/Micro Engineered and Molecular Systems*, pp.1067-1070, Jan. 2008.

[26] C. Junseok, H. Kulah, K. Najafi, "A monolithic three-axis micro-g micromachined silicon capacitive accelerometer", *Journal of Microelectromechanical Systems*, vol.14, no.2, pp. 235- 242, Apr. 2005.

[27] C. M. Sun, M.H. Tsai, W. Fang, "Design and Implementation of a Novel CMOS-MEMS Single Proof-Mass Tri-Axis Accelerometer", *MEMS 2009. IEEE 22nd International Conference on Micro Electro Mechanical Systems, 2009*, pp.809-812, Jan. 2009.

[28] H. Jung-Tang, L. Chieh-Han, Y. Chiu-Chin, J. Kai-Yuan, L. Jeng, L. Kuo-Yu , "The 3-axis CMOS-MEMS accelerometer include accelerator sensing method of Z-axis", *EMAP 2008. International Conference on Electronic Materials and Packaging, 2008*, pp.321-324, 22-24 Oct. 2008

[29] X. Huikai and G.K. Fedder, "A CMOS z-axis capacitive accelerometer with comb-finger sensing", *MEMS 2000. The Thirteenth Annual International Conference on Micro Electro Mechanical Systems*, pp.496-501, Jan 2000.

[30] "ADXL203 Precision 1.7g Dual-Axis iMEMS Accelerometer" Analog Devices. Web. 24 Nov. 2010. <http://www.analog.com/en/sensors/inertial-sensors/adxl203/products/product.html>

[31] "STMicroelectronics MEMS intertial sensor 3-axis ultracompact linear accelerometer" STMicroelectronics. Web. 24 Nov 2010. <http://www.st.com/stonline/products/literature/ds/14282/lis344al.htm>

[32] G.K. Fedder. 1994. "Simulation of Microelectromechanical Systems". Ph.D. dissertation, Carnegie Mellon University.

[33] G. Zhang, H. Xie, L.E. de Rosset, G.K. Fedder, "A lateral capacitive CMOS accelerometer with structural curl compensation", *MEMS '99. Twelfth IEEE International Conference on Micro Electro Mechanical Systems*, pp.606-611, Jan. 1999.

[34] MATLAB version 7.6.0 R2008. Natick, Massachusetts: The MathWorks Inc., 2008.

[35] "Coventor Inc." Coventorware Suite, 2008, Cary, NC. [Online]. Available: <http://www.coventor.com/coventorware.html>

Appendix 1

Matlab code for analytical exploration

Explore.m

```
dim1=1; dim2=1; dim3=1; dim4=1; dim5=1;
kxt=0; kzt=0; freqt=0; frext=0;
ranget=0; crosst=0; freqt=0; areat=0;
m=2.42E-09;

for n=3:2:7
  dim4=1;
  for wa=0.5:0.5:20
    dim3=1;
    for wb=0.5:0.5:20
      dim2=1;
      for atemp=2:1:50
        dim1=1;
        for b=40:5:290

          [kz,kx]=rigidez(n,atemp,b,wa,wb);
          kxt(dim5,dim3,dim1,dim4,dim2)=kx;
          kzt(dim5,dim3,dim1,dim4,dim2)=kz;
          freq=sqrt(kz/m)/(2*3.1416);
          freqt(dim5,dim3,dim1,dim4,dim2)=freq;
          frex=sqrt(kx/m)/(2*3.1416);
          frext(dim5,dim3,dim1,dim4,dim2)=frex;
          area=(1.4142*400e-6+(n*atemp*1e-6+120e-6)*2)*(1.4142*400e-6+(n*atemp*1e-6+120e-6)*2);
          areat(dim5,dim3,dim1,dim4,dim2)=area*1000000;
          range=(kz*1.7e-6)/(m*9.7976);
          ranget(dim5,dim3,dim1,dim4,dim2)=range;
          cross=kz/kx;
          crosst(dim5,dim3,dim1,dim4,dim2)=cross;
          dim1=dim1+1;
          end
        dim2=dim2+1;
      end
      dim3=dim3+1;
    end
    dim4=dim4+1;
    wa
  end
  dim5=dim5+1;
end
```

Rigidez.m

```
function [kzTot,kxTot] = rigidez(n,atemp,b,wa,wb)

t=1.31; a=atemp;
a=a*1e-6;
b=b*1e-6;
t=t*1e-6;
```

```
wa=wa*1e-6;
wb=wb*1e-6;

E=73.55e9; v=0.3;
G=E/(2*(1+v));
Iza=t.*wa.^3/12;
Izb=t.*wb.^3/12;
a_raya=Izb*a/Iza;
Ixa=wa.*t.^3/12;
Ixb=wb.*t.^3/12;
if(wa>t)
   Ja=wa*t^3*(1/3-0.21*t/wa*(1-t^4/(12*wa^4)));
else
   Ja=t*wa^3*(1/3-0.21*wa/t*(1-wa^4/(12*t^4)));
end

if(wb>t)
   Jb=wb*t^3*(1/3-0.21*t/wb*(1-t^4/(12*wb^4)));
else
   Jb=t*wb^3*(1/3-0.21*wb/t*(1-wb^4/(12*t^4)));
end

Sea=E*Ixa;
Seb=E*Ixb;
Sga=G*Ja;
Sgb=G*Jb;

kx=48*E*Izb/(a^2*n*((a_raya+b)*n^2-3*b*n+2*b));
ky=48*E*Izb*((a_raya+b)*n-b)/(b^2*(n-1)*((3*a_raya^2+4*a_raya*b+b^2)*n+3*a_raya^2-b^2));
kz=48*Sea*Seb*Sga*Sgb*(Sga*b*(n-1)+Seb*a*n)/(Seb*Sga*a^2*(Seb*Sgb*a^2+(Sea*Seb+Sga*Sgb)*a*b+Sea*Sga*b^2)*n^4-
Seb*Sga*a^2*b*((3*Sea*Seb+Sga*Sgb)*a+4*Sea*Sga*b)*n^3+Sea*b*(2*Seb^2*Sga*a^3+(5*Seb*Sga^2+3*Seb^2*Sgb)*a^2*b+4*Seb*Sga*
Sgb*a*b^2+Sga^2*Sgb*b^3)*n^2-2*Sea*Sga*b^2*(Seb*Sga*a^2+2*Seb*Sgb*a*b+Sga*Sgb*b^2)*n+Sea*Sgb*b^2*(Sga^2*b^2-
3*Seb^2*a^2));

frex=sqrt(kx/1.8588e-9)/(2*3.1416);
frey=sqrt(ky/1.8588e-9)/(2*3.1416);
frez=sqrt(kz/1.8588e-9)/(2*3.1416);

kxTot=kx+ky;
kzTot=2*kz;

end
```

Appendix 2

AIM code for synthesis program

Synth.aim

```
proc MyFun:Loop {value obcross obarea}  {

global MyFun
set type $MyFun(f3)
global t

if ([string match $type " kz (n/m)   5e-4 - 14 n/m  "]) then {
set type 0
} else {
if ([string match $type " resonance frequency (hz)   70 - 12,000 hz "]) then {
set type 1
} else {
set type 2
}
}

if {![isvalid double $value]} {

if ($type==0) then {
AimMessage "The specified stiffness must be a valid floating point number" error
} else {
if (type==1) then {
AimMessage "The specified frequency must be a valid floating point number" error
} else {
AimMessage "The specified range must be a valid floating point number" error
}
}
    return
  }
if {![isvalid double $obcross]} {
    AimMessage "The specified cross-axis sensitivity must be a valid floating point number" error
return
  }
if {![isvalid double $obarea]} {
    AimMessage "The specified area must be a valid floating point number" error
    return
  }

if ($type==0) then {
if ($value<3e-4|$value>10) {
AimMessage "The specified stiffness must be within the range 3e-4 - 10 N/m  " error
return
}
} else {
if ($type==1) then {
if ($value<50|$value>11000) {
AimMessage "The specified frequency must be within the range 50 - 11,000 Hz  " error
return
}
```

```
} else {
if ($value<0.2|$value>800) {
AimMessage "The specified minimum acceleration range must be within the range 0.20 - 800 G  " error
return
}
}
}

if ($obcross<6e-5|$obcross>0.5) {
AimMessage "The specified cross-axis sensitivity must be within the range 6e-5 - 0.5  " error
return
}
if ($obarea<0.66|$obarea>2.26) {
AimMessage "The specified cross-axis sensitivity must be within the range 0.66 - 2.26 mm^2  " error
return
}


set finala 0
set finalwa 0
set finalb 0
set finalwb 0
set finaln 0

set found 0
set foundkz 0
set foundrange 0
set foundfreq 0
set foundcross 0
set foundarea 0

set nearkz 0
set nearrange 0
set nearfreq 0
set nearcross 0
set neararea 0

set first 0

for {set n 3} {$n < 9} {let n=$n+2} {

for {set wa 0.5} {$wa < 20.5} {let wa=$wa+0.5} {

for {set wb 0.5} {$wb < 20.5} {let wb=$wb+0.5} {

for {let atemp=$wb*2+0.5} {$atemp<50} {let atemp=$atemp+5} {

for {set b 40} {$b < 280} {let b=$b+20} {

array set stiff [MyFun.Cal $n $atemp $b $wa $wb]
let kz=$stiff(kz)*2
let kx=$stiff(kx)+$stiff(ky)
let range=$kz*1.7e-6/(9.8*(2.42e-09))
let freq=sqrt($kz/(2.42e-09))/(2*3.1416)
let cross=$kz/$kx
let area=(1.4142*400e-6+($n*$atemp*1e-6+120e-6)*2)*(1.4142*400e-6+($n*$atemp*1e-6+120e-6)*2)
puts "Rango $range kz $kz kx $kx cross $cross N $n a $atemp b $b wa $wa wb $wb"

if ($type==0)  then {

let err=($kz-$value)/$value
let err=abs($err)
if {($err<0.01)&($cross<=$obcross)&($area<=$obarea)} then {
set finalb $b
set found 1
} else {

if {($cross<=$obcross)&($area<=$obarea)} then {
let comp1=abs($kz-$value)
let comp2=abs($nearkz-$value)
```

```
if {($comp1)<($comp2)} {
set nearkz $kz
set nearrange $range
set nearfreq $freq
set nearcross $cross
set neararea $area
if ($first==0) then {
set first 1
}
}
}
}

} else {
if ($type==1) then {

let err=($freq-$value)/$value
let err=abs($err)

if {($err<0.01)&($cross<=$obcross)&($area<=$obarea)} then {

set finalb $b
set found 1
} else {

if {($cross<=$obcross)&($area<=$obarea)} then {

let comp1=abs($freq-$value)
let comp2=abs($nearfreq-$value)
if {($comp1)<($comp2)} {
set nearkz $kz
set nearrange $range
set nearfreq $freq
set nearcross $cross
set neararea $area
if ($first==0) then {
set first 1
}
}
}
}
} else {

let err=($range-$value)/$value
let err=abs($err)
if {($err<0.01)&($cross<=$obcross)&($area<=$obarea)} then {
set finalb $b
set found 1
} else {

if {($cross<=$obcross)&($area<=$obarea)} then {

let comp1=abs($range-$value)
let comp2=abs($nearrange-$value)
if {($comp1)<($comp2)} {
set nearkz $kz
set nearrange $range
set nearfreq $freq
set nearcross $cross
set neararea $area
if ($first==0) then {
set first 1
}
}
}
}
}
}
```

```
if {$found==1} then {
puts "Found range $range kz $kz cross $cross N $n a $atemp b $b wa $wa wb $wb"
set finalb $b
set foundkz $kz
set foundrange $range
set foundfreq $freq
set foundcross $cross
set foundarea $area
break
}
}
if {$found==1} then {
set finala $atemp
break
}
}
if {$found==1} then {
set finalwb $wb
break
}
}
if {$found==1} then {
set finalwa $wa
break
}
}
if {$found==1} then {
set finaln $n
break
}
}

let finala=$finala*1e-6
let finalwa=$finalwa*1e-6
let finalb=$finalb*1e-6
let finalwb=$finalwb*1e-6


set MyFun(finala) $finala
set MyFun(finalwa) $finalwa
set MyFun(finalb) $finalb
set MyFun(finalwb) $finalwb
set MyFun(finaln) $n

destroy $t.f1.f7
destroy $t.f1.f8
destroy $t.f1.f9
destroy $t.f1.f10
destroy $t.f1.f11
destroy $t.f1.f12

frame $t.f1.f7
   pack $t.f1.f7 -side top -expand yes -fill both -pady 2
   entry $t.f1.f7.e -textvariable MyFun(text)
   pack $t.f1.f7.e -side left -expand yes -fill both -padx 2

frame $t.f1.f8
   pack $t.f1.f8 -side top -expand yes -fill both -pady 2
   entry $t.f1.f8.e -textvariable MyFun(textkz)
   pack $t.f1.f8.e -side left -expand yes -fill both -padx 2

frame $t.f1.f9
   pack $t.f1.f9 -side top -expand yes -fill both -pady 2
   entry $t.f1.f9.e -textvariable MyFun(textfreq)
   pack $t.f1.f9.e -side left -expand yes -fill both -padx 2

frame $t.f1.f10
   pack $t.f1.f10 -side top -expand yes -fill both -pady 2
   entry $t.f1.f10.e -textvariable MyFun(textrange)
   pack $t.f1.f10.e -side left -expand yes -fill both -padx 2
```

```
frame $t.f1.f11
  pack $t.f1.f11 -side top -expand yes -fill both -pady 2
  entry $t.f1.f11.e -textvariable MyFun(textarea)
  pack $t.f1.f11.e -side left -expand yes -fill both -padx 2

frame $t.f1.f12
  pack $t.f1.f12 -side top -expand yes -fill both -pady 2
  entry $t.f1.f12.e -textvariable MyFun(textcross)
  pack $t.f1.f12.e -side left -expand yes -fill both -padx 2


if {$found==1} then {
set MyFun(text) "Performance values of synthetized accelerometer:"
set MyFun(textkz) "kz $foundkz N/m"
set MyFun(textfreq) "Resonance frequency: $foundfreq Hz"
set MyFun(textrange) "Acceleration Range: $foundrange g"
set MyFun(textarea) "Area: $foundarea mm^2"
set MyFun(textcross) "Cross Sensitivity: $foundcross"

destroy $t.f1.f14


frame $t.f1.f14
pack $t.f1.f14 -side top -expand yes -fill both -pady 4
button $t.f1.f14.b1 -text "Generate Layout"  -command "AimBusy  {MyFun:Layout}  {. $t} watch"
button $t.f1.f14.b3 -text "Close"  -command "MyFun:Close"
pack $t.f1.f14.b1 $t.f1.f14.b3 -side left  -expand yes -fill both -padx 5

} else{
if ($first==0) then {
set MyFun(text) "A design meeting the minimum cross axis sensitivity and maximum area requirements could not be found"
set MyFun(textkz) ""
set MyFun(textfreq) ""
set MyFun(textrange) ""
set MyFun(textarea) ""
set MyFun(textcross) ""
set first 1
} else {

set MyFun(text) "The closest design found has the following performance values :"
set MyFun(textkz) "kz $nearkz"
set MyFun(textfreq) "Resonance frequency: $nearfreq"
set MyFun(textrange) "Acceleration Range: $nearrange"
set MyFun(textarea) "Area: $neararea"
set MyFun(textcross) "Cross Sensitivity: $nearcross"

destroy $t.f1.f14

frame $t.f1.f14
pack $t.f1.f14 -side top -expand yes -fill both -pady 4
button $t.f1.f14.b1 -text "Generate Layout"  -command "AimBusy  {MyFun:Layout}  {. $t} watch"
button $t.f1.f14.b3 -text "Close"  -command "MyFun:Close"
pack $t.f1.f14.b1 $t.f1.f14.b3 -side left  -expand yes -fill both -padx 5
}
}



}

proc MyFun:Cal {n atemp b wa wb}  {

set t 1.31
let a=$atemp
let a=$a*1e-6
let b=$b*1e-6
let t=$t*1e-6
let wa=$wa*1e-6
```

```
let wb=$wb*1e-6

let E=73.55e9
let v=0.3
let G=$E/(2*(1+$v))
let Iza=$t*$wa*$wa*$wa/12
let Izb=$t*$wb*$wb*$wb/12
let araya=$Izb*$a/$Iza
let Ixa=$wa*$t*$t*$t/12
let Ixb=$wb*$t*$t*$t/12

if {$wa>$t} then {
let Ja=$wa*$t*$t*$t*(1.0/3-0.21*$t/$wa*(1-$t*$t*$t*$t/(12*$wa*$wa*$wa*$wa)))
} else {
let Ja=$t*$wa*$wa*$wa*(1.0/3-0.21*$wa/$t*(1-$wa*$wa*$wa*$wa/(12*$t*$t*$t*$t)))
}

if {$wb>$t} then {
let Jb=$wb*$t*$t*$t*(1.0/3-0.21*$t/$wb*(1-$t*$t*$t*$t/(12*$wb*$wb*$wb*$wb)))
} else {
let Jb=$t*$wb*$wb*$wb*(1.0/3-0.21*$wb/$t*(1-$wb*$wb*$wb*$wb/(12*$t*$t*$t*$t)))
}

let Sea=$E*$Ixa
let Seb=$E*$Ixb
let Sga=$G*$Ja
let Sgb=$G*$Jb
let kx=48*$E*$Izb/($a*$a*$n*(($araya+$b)*$n*$n-3*$b*$n+2*$b))
let ky=48*$E*$Izb*(($araya+$b)*$n-$b)/($b*$b*($n-1)*((3*$araya*$araya+4*$araya*$b+$b*$b)*$n+3*$araya*$araya-$b*$b))
let kz=48*$Sea*$Seb*$Sga*$Sgb*($Sga*$b*($n-
1)+$Seb*$a*$n)/($Seb*$Sga*$a*$a*($Seb*$Sgb*$a*$a+($Sea*$Seb+$Sga*$Sgb)*$a*$b+$Sea*$Sga*$b*$b)*$n*$n*$n*$n-
$Seb*$Sga*$a*$a*$b*((3*$Sea*$Seb+$Sga*$Sgb)*$a+4*$Sea*$Sga*$b)*$n*$n*$n+$Sea*$b*(2*$Seb*$Seb*$Sga*$a*$a*$a+(5*$Seb*$Sga
*$Sga+3*$Seb*$Seb*$Sgb)*$a*$a*$b+4*$Seb*$Sga*$Sgb*$a*$b*$b+$Sga*$Sga*$Sgb*$b*$b*$b)*$n*$n-
2*$Sea*$Sga*$b*$b*($Seb*$Sga*$a*$a+2*$Seb*$Sgb*$a*$b+$Sga*$Sgb*$b*$b)*$n+$Sea*$Sgb*$b*$b*($Sga*$Sga*$b*$b-
3*$Seb*$Seb*$a*$a))

set stiff(kx) $kx
set stiff(ky) $ky
set stiff(kz) $kz
array get stiff
}


proc MyFun:Layout {} {

global MyFun

if ($MyFun(finaln)==3) then {
SchMgr:SchDesign TesisN3.ai_sch C:/Coventor/Design_Files/Gyroscope/Schematics
} else {
if ($MyFun(finaln)==5) then {
SchMgr:SchDesign TesisN5.ai_sch C:/Coventor/Design_Files/Gyroscope/Schematics
} else {
SchMgr:SchDesign TesisN7.ai_sch C:/Coventor/Design_Files/Gyroscope/Schematics
}
}

sch property saber_2_ value -name largo2 $MyFun(finalb)
sch property saber_2_ value -name ancho2 $MyFun(finalwb)
sch property saber_2_ value -name largo3 $MyFun(finala)
sch property saber_2_ value -name ancho3 $MyFun(finalwa)
sch write -force
}

proc MyFun:Open {} {

SchMgr:SchDesign TesisN7.ai_sch C:/Coventor/Design_Files/Gyroscope/Schematics


sch property saber_2_ value -name largo2 200u
```

```
sch property saber_2_ value -name ancho2 15u
sch property saber_2_ value -name largo3 20u
sch property saber_2_ value -name ancho3 10u

sch write -force


}

# This proc creates the toplevel form
proc MyFun:Create {} {

   global MyFun homeDirectory
global t
   set t .ss
   if {[winfo exists $t]} {
destroy $t
   }

   toplevel $t
   set MyFun(root) $t
   Aim:SetToolOrigin $t
   wm title $t {CMOS MEMS Z-axis Accelerometer Synthesis}



   if {![info exists MyFun(frequency)]} {
      set MyFun(frequency) "10"
   }
   if {![info exists MyFun(cross)]} {
set MyFun(cross) "10"
   }

set MyFun(text) ""
   set MyFun(textkz) ""
set MyFun(textfreq) ""
set MyFun(textrange) ""
set MyFun(textarea) ""
set MyFun(textcross) ""


   frame $t.f1  -relief groove  -borderwidth 2
   pack $t.f1 -side top -expand yes -fill both


# frame for checkbutton
AimForm:LabelChoice $t.f1.f2 -name "Choose a performance variable" \
-var MyFun(f3) \
-choiceList  {{ kz (N/m)   5e-4 - 14 N/m  } { Resonance frequency (Hz)   70 - 12,000 Hz } { Maximum Acceleration (G)  0.04 - 1000 G }} \
-choiceType togglebutton -nopack 1 -borderwidth 5


   frame $t.f1.f3
   pack $t.f1.f2  $t.f1.f3 -side top -expand yes -fill both -pady 2
   label $t.f1.f3.l -text "Value"  -width 40  -anchor w
   pack $t.f1.f3.l -side left -expand no
   entry $t.f1.f3.e -textvariable MyFun(value)  -borderwidth 2  -relief sunken
   pack $t.f1.f3.e -side left -expand yes -fill both

frame $t.f1.f4
   pack $t.f1.f4 -side top -expand yes -fill both -pady 2
   label $t.f1.f4.l -text "Maximum Cross Axis Sensitivity: 6e-5 - 1.16 "  -width 40  -anchor w
   pack $t.f1.f4.l -side left -expand no
   entry $t.f1.f4.e -textvariable MyFun(cross)  -borderwidth 2  -relief sunken
   pack $t.f1.f4.e -side left -expand yes -fill both -padx 2

frame $t.f1.f5
   pack $t.f1.f5 -side top -expand yes -fill both -pady 2
   label $t.f1.f5.l -text "Maximum Area: 0.66 - 2.26 mm^2"  -width 40  -anchor w
   pack $t.f1.f5.l -side left -expand no
```

```
   entry $t.f1.f5.e -textvariable MyFun(area)  -borderwidth 2  -relief sunken
   pack $t.f1.f5.e -side left -expand yes -fill both -padx 2



   frame $t.f1.f6
   pack $t.f1.f6 -side top -expand yes -fill both -pady 4
   button $t.f1.f6.b1 -text "Start Synthesis"  -command "AimBusy  {MyFun:Loop \$MyFun(value) \$MyFun(cross) \$MyFun(area) }  {. $t}
watch"
   button $t.f1.f6.b3 -text "Close"  -command "MyFun:Close"
   pack $t.f1.f6.b1 $t.f1.f6.b3 -side left  -expand yes -fill both -padx 5
   return {}
}

proc MyFun:Close {} {
   global MyFun

   destroy $MyFun(root)
}
```